Ecological Modelling 436 (2020) 109292

Contents lists available at ScienceDirect

Ecological Modelling

journal homepage: www.elsevier.com/locate/ecolmodel

Modeling soil porewater salinity in mangrove forests (Everglades, Florida, USA) impacted by hydrological restoration and a warming climate

Xiaochen Zhao[a,*], Victor H. Rivera-Monroy[a], Hongqing Wang[b], Z George Xue[a,c,d], Cheng-Feng Tsai[e], Clinton S. Willson[e], Edward Castañeda-Moya[f], Robert R. Twilley[a]

[a] Department of Oceanography and Coastal Sciences, College of the Coast and Environment, Louisiana State University, Baton Rouge, LA70803, United States
[b] U.S. Geological Survey Wetland and Aquatic Research Center, Baton Rouge, LA70803, United States
[c] Center for Computation and Technology,Louisiana State University, Baton Rouge, LA70803, United States
[d] Coastal Studies Institute, Louisiana State University, Baton Rouge, LA70803, United States
[e] Department of Civil and Environmental Engineering, College of Engineering, Louisiana State University, Baton Rouge, LA70803, United States
[f] Southeast Environmental Research Center, Institute of Environment, Florida International University,Miami, FL33199, United States

ARTICLE INFO

Keywords:
Florida Everglades mangrove wetlands
Porewater salinity
Mass balance
Water and salt budgets
Hydrological restoration
Climate change

ABSTRACT

Hydrology is a critical driver controlling mangrove wetlands structural and functional attributes at different spatial and temporal scales. Yet, human activities have negatively affected hydrology, causing mangrove die-backs and coverage loss worldwide. In fact, the assessment of mangrove water budgets, impacted by natural and human disturbances, is limited due to a lack of long-term data and information that hinders our understanding of how changes in hydroperiod and salinity control mangrove productivity and spatial distribution. In this study, we implemented a mass balance-based hydrological model (RHYMAN) that explicitly considers groundwater discharge in the Shark River estuary (SRE, southwestern Everglades) located in a karstic geomorphic setting and influenced by regional hydrological restoration. We used long-term hydroperiod and porewater salinity (PWS) datasets obtained from 2004 to 2016 for model calibration and validation and to determine spatiotemporal variability in water levels and PWS at three riverine mangrove sites (downstream, SRS-6; midstream, SRS-5; upstream, SRS-4) along SRE. Model results agree with a distinct PWS pattern along the estuarine salinity gradient where the highest PWS occurs at SRS-6 (mean: 25, range: 22–30 ppt), followed by SRS-5 (17, 14–25 ppt) and SRS-4 (5, 3–13 ppt). A commensurate increase in PWS over a thirteen-year period indicates a long-term reduction in freshwater inflow coupled with sea-level rise (SLR). Increasing freshwater scenario simulation results show a significant reduction (17–27%) in PWS along the estuary in contrast with a high SLR scenario when salinity increases up to 1.1 to 2.5 times that of control values. Model results show that freshwater inflow and SLR are key drivers controlling mangrove wetlands PWS in this karstic coastal region. Given its relatively simple structure, this mass balance-based hydrological model could be used in other environmental settings to evaluate potential habitat and regime shifts due to changes in hydrology and PWS under regional hydrological restoration management.

1. Introduction

Mangrove wetlands are distributed along low-latitude intertidal zones. Although mangrove wetlands account for only 0.7% of the tropical forest area, they are recognized as the most productive ecosystems per unit area in the world (Donato et al., 2011; Giri et al., 2011). Mangrove forests structure and productivity are regulated by the interaction among a range of abiotic factors including global climate (i.e., temperature and precipitation), regional coastal geomorphology and local hydrological processes across multiple spatiotemporal scales (Rivera-Monroy et al., 2017; Rovai et al., 2016; Twilley et al., 2017; Twilley and Rivera-Monroy, 2005). Indeed, hydrology is recognized as "the single most important determinant" in establishing and maintaining the structure and biogeochemical processes in wetlands (Mitsch and Gosselink, 2007).

In mangrove-dominated coastal wetlands, hydrological processes, including tide, surface sheet flow, precipitation, evapotranspiration, and groundwater, determine water budget of the ecosystems. Therefore, the water budget defines a critical local hydrological signature represented by the hydroperiod (frequency, duration, and depth

* Corresponding author.
E-mail address: xzhao24@lsu.edu (X. Zhao).

https://doi.org/10.1016/j.ecolmodel.2020.109292
Received 10 March 2020; Received in revised form 11 September 2020; Accepted 13 September 2020

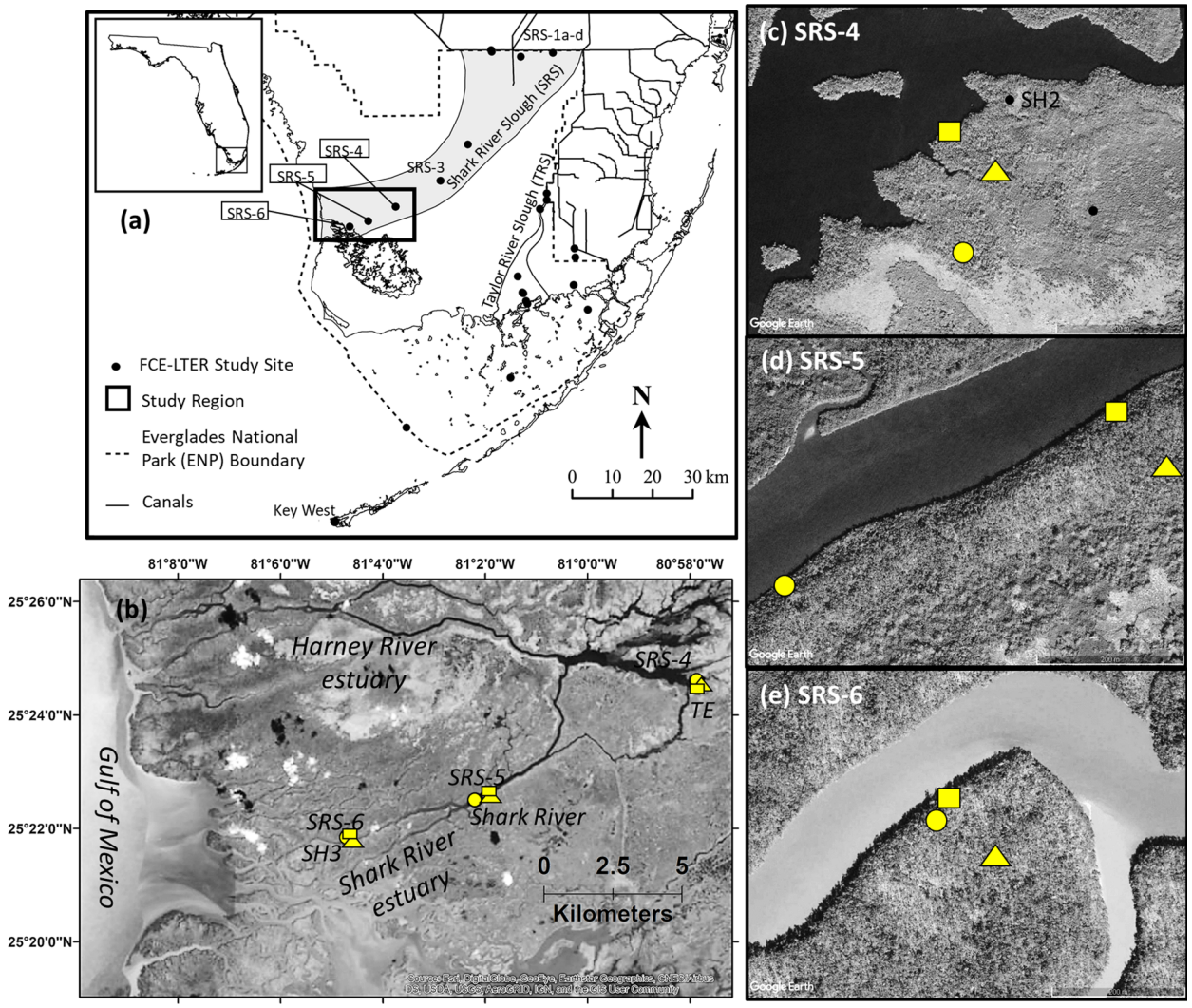

Fig. 1. (a) Shark River and Taylor River Sloughs (SRS and TRS) location across the Everglades National Park (ENP), South Florida. (b) Shark River and Harney River estuaries. (c-e) study sites located along Shark River estuary from upstream (SRS-4) to midstream (SRS-5) and downstream (SRS-6) regions. Circle: U.S. Geological Survey (USGS) precipitation and evapotranspiration (ET) station; rectangle: Florida Coastal Everglades Long Term Ecological Research (FCE LTER) channel water level recorder; triangle: FCE LTER forest water level recorder.

of inundation). Hydroperiod interacts with both resource availability (e.g., nutrients, space, and light) and stressor gradients (e.g., salinity, sulfides) that determine the relative dominance of mangrove ecotypes (i.e., scrub, basin, riverine and fringe; Lugo and Snedaker, 1974) and reflect a range of potential forest structure (e.g., tree height, stand density) and net primary productivity (NPP) patterns (Lugo and Snedaker, 1974; Rivera-Monroy et al., 2019; Rovai et al., 2018). Further, these structural and productivity differences are modulated by dominant mangrove species-specific physiological adaptations (i.e., *Avicennia germinans, Laguncularia racemosa, Rhizophora mangle*) in neotropical latitudes that are based on different species strategies to cope with the complex interactions among hydroperiod and resource and stressor gradients (Lugo and Snedaker, 1974; Rivera-Monroy et al., 2017; Twilley et al., 2017; Twilley and Rivera-Monroy, 2005). Mangrove species, for instance, can grow in a wide range of soil porewater salinity (PWS), from freshwater to about three times that of seawater salinity (i.e., 90 ppt); in particular some species require relatively higher PWS for maximum growth and competitive advantage (Ball, 1988a, 1988b; Krauss et al., 2008; Lugo and Medina, 2014). In coastal wetlands, this typical brackish-saline condition controls PWS as a result of the dynamic water and material exchanges with seawater through tidal cycles among other hydrological processes that define the hydroperiod gradient. Hence, PWS is considered as a major driver not only regulating species composition, tree height and NPP along well-defined mangrove zones as a result of inter- and intra-species competition given species-specific salinity tolerance (Ball and Pidsley, 1995; Castañeda-Moya et al., 2006; Crase et al., 2013; Day et al., 1996; Kauffman and Bhomia, 2017; Mitsch and Gosselink, 2007; Rivera-Monroy et al., 2017; Simard et al., 2019), but also affecting belowground microbial activities and biogeochemistry, which directly impact soil fertility and carbon budgets in mangrove soils (Alongi et al., 1993; Bouillon et al., 2007; Chambers et al., 2016; Kristensen et al., 2017; Lee et al., 2008; McKee et al., 1988; Sherman et al., 1998; Troxler et al., 2015). Despite the crucial role of PWS on mangrove ecological attributes, there is a lack of long-term continuous field data to determine PWS seasonal and interannual variability, particularly in subtropical and arid coastal mangrove wetlands (Kristensen et al., 2017). Time- and labor-consuming field sampling due to the forest structure complexity (e.g., dense prop roots) under flooding conditions and hard access to the remote sites along the coastal zone are some of the reasons for this data gap.

Because PWS is regulated by the net exchange of salt between mangrove forests and adjacent coastal waters, hydrological models are useful analytical tools to examine water budgets that determine

seasonal and interannual PWS variability in mangroves. Although existing hydrodynamic models are capable of reproducing water flows in mangrove forests (Alongi, 2009; Mazda et al., 2005), these models are not able to explicitly predict changes in PWS. This limitation is associated with the complex interplay among mangrove hydrological conditions, groundwater, and sea level rise (SLR) (Dessu et al., 2018; Nuttle et al., 2000; Price et al., 2006; Saha et al., 2011; 2012). Increasing freshwater inflows, for example, controlled by river and groundwater discharge due to restoration diversions, can lead to fresher groundwater, while SLR causes saltwater intrusion (Habib et al., 2007; 2008; Michot et al., 2017; Saha et al., 2011). Therefore, depending on the geomorphic setting (e.g., karstic vs deltaic; Rovai et al., 2016; 2018; Woodroffe, 2002) and the relative dominance of groundwater discharge and SLR, this complex interaction among environmental settings causes uncertainties in the assessment of PWS, especially when site-specific parameterization is constrained by data with limited sampling spatial coverage and frequency. Although modeling studies have been conducted to evaluate hydrological processes and salinity in estuaries or tidal creeks adjacent to mangrove wetlands (Langevin et al., 2005; Michot et al., 2017; Wang et al., 2012), few studies have explicitly partitioned the difference between water column salinity and PWS (Chen and Twilley, 1999; He et al., 2020; Lara and Cohen, 2006; Leopold et al., 2017; Sherman et al., 1998; Simard et al., 2019), or attempted to forecast mangrove PWS patterns (e.g., Tsai, 2008; Twilley and Chen, 1998).

The overall objective of this study is to evaluate seasonal and interannual PWS variability in riverine mangrove forests in the Everglades Mangrove Ecotone Region (EMER; Rivera-Monroy et al., 2011) along the Shark River estuary (SRE; southwestern Florida) using a mass balance-based hydrological model which was modified from the previous MANgrove HYdrological model (hereafter, HYMAN; Twilley and Chen, 1998). Surface freshwater and groundwater flow are highly regulated along the Shark River Slough (SRS) and Taylor River Slough (TRS) (**Fig. 1**) as part of the Comprehensive Everglades Restoration Plan (CERP; National Academies of Sciences, 2016) and in the context of the Everglades National Park (ENP) conservation and management program (Sklar et al., 2005). Increasing freshwater inflows to the SRE under the CERP management will modify both estuarine water column depth and groundwater discharge, therefore reducing mangrove PWS, which can potentially lead to changes in resource competition (e.g., nutrient, light, space) between freshwater vegetation and mangrove wetlands, especially at the upstream EMER (Dessu et al., 2018). In contrast, due to the rapid increase in SLR associated with climate change in South Florida over the last decade (Dahl et al., 2017; Flower et al., 2019; Saha et al., 2011; Wdowinski et al., 2016), there is significant saltwater intrusion along the coast, including the SRE and Florida Bay (Dessu et al., 2018; Nuttle et al., 2000; Price et al., 2006; Saha et al., 2012). In combination with a potential increase in nutrient inputs from the Gulf of Mexico during hurricanes (Castañeda-Moya et al., 2010; 2020) along with SLR, PWS changes may further increase the replacement of brackish marshes with mangrove forests along both the SRS and TRS (Ewe et al., 2007; Han et al., 2018; Howard et al., 2017; Troxler et al., 2013).

To our best knowledge, HYMAN is still the only mass balance model targeted for mangrove forests and it is a useful tool to forecast mangrove forest water budgets and PWS with relatively low uncertainty (Tsai, 2008; Twilley and Chen, 1998). However, HYMAN was initially calibrated and validated for basin mangrove forests in Rookery Bay, South Florida (Twilley and Chen, 1998), and it did not explicitly include groundwater processes, a critical water budget component especially in karstic coastal regions like South Florida (Price et al., 2006; Saha et al., 2012; Tobias et al., 2001). Given the current and projected changes in freshwater restoration and SLR across the EMER, we further advanced the HYMAN model, as the Riverine MANgrove HYdrological model (hereafter, RHYMAN, **Fig. 2**) given the structural modifications. We conducted model calibration and validation using long-term data (2004–2016) collected at riverine mangrove sites along the SRE. RHYMAN explicitly includes two groundwater sources: the upstream fresh groundwater discharge (FGD) influenced by freshwater restoration projects and the coastal groundwater discharge (CGD) caused by rising sea level. The specific objectives of this paper are to: (1) implement a mass balance-based hydrological model for riverine mangroves that explicitly considers groundwater inputs in a karstic coastal region and (2) evaluate PWS spatiotemporal variation under different scenarios defined by variable upstream freshwater inflow and SLR.

2. Materials and methods

2.1. Study sites

Mangrove extension in the Everglades National Park, South Florida is ~1444 km^2 and dominated by three mangrove species, *Rhizophora mangle*, *Laguncularia racemosa*, and *Avicennia germinans*, and one associated species, *Conocarpus erectus*, restricted to upstream parts of mangrove-dominated estuaries (**Fig. 1a**) (Castañeda-Moya et al., 2013; Childers, 2006; Rivera-Monroy et al., 2011). The Shark River estuary (SRE; **Fig. 1b**) lies along the lower Shark River Slough (SRS) in the southwestern region where semidiurnal tides are dominant (tidal range: 1.1 m; Provost, 1973). This Everglades forested wetland provides valuable ecosystem services (i.e., carbon storage) with an estimated cumulative value ranging from $2 −3.4 billion in 2015 US$ (Jerath et al., 2016). Along the SRE, three mangrove-dominated study sites (**Fig. 1c-e**) were established from downstream (SRS-6) to mid- and upstream (SRS-5, SRS-4) regions along the estuary, as part of the Florida Coastal Everglades Long Term Ecological Research program since 2001 (FCE LTER; http://fcelter.fiu.edu/) (Childers, 2006). Seventy percent of the average annual precipitation (~1500 mm) in South Florida falls during the wet season (Duever et al., 1994). The average annual evapotranspiration is approximately 1400 mm with half occurring in the dry season (December to mid-June) and the rest in the wet season (mid-June to November). Two permanent plots (20 m × 20 m) were established at each site and sampled at least once in the wet and dry seasons per year from 2002 to 2016. PWS was measured at 30-cm soil depth using a handheld YSI sonde (model 30, YSI Incorporated, Yellow Springs, Ohio) at four sampling stations systematically located within each plot. One ultrasonic water level recorder (INFINITIES-USA INC.) was installed at each site to monitor hourly water levels relative to the forest soil surface; instrument location inside the forest was 70 m (SRS-4, SRS-5) and 60 m (SRS-6) from the shoreline (**Fig. S1**). Further details about sampling techniques are described in Castañeda-Moya et al. (2013). Overall, the three study sites are characterized by distinct mangrove structural and functional properties influenced by soil total phosphorous (TP) (range: 0.05–0.20 mg cm^{-3}), PWS (4–26 ppt), flooding duration (3965–5592 hour yr^{-1}) and frequency (165–395 tides yr^{-1}) gradients (Castañeda-Moya et al., 2013; 2020; Chen and Twilley, 1999). Average mangrove tree height generally decreases from the downstream (~18 m) to upstream (<~6 m; Simard et al., 2006; 2019). Due to differences in soil nutrients, PWS, and hydroperiod regimes, mangrove species dominance varies among sites: *L. racemosa* dominates in SRS-6, while *R. mangle* dominates in SRS-5 and SRS-4. The upstream (SRS-4) site marks the boundary of the mangrove-saltmarsh ecotone where freshwater and brackish vegetation are present (Danielson et al., 2017; Rivera-Monroy et al., 2019).

2.2. Model description

Tide, precipitation, surface sheet flow, groundwater, seepage, and evapotranspiration are the main drivers controlling the hydrological processes in mangrove wetlands (Mitsch and Gosselink, 2007; Twilley and Chen, 1998). The spatiotemporal interactions among those drivers control the exchange of water and salt between mangroves and adjacent estuarine waters and upland ecosystems (**Fig. 2**). We adapted

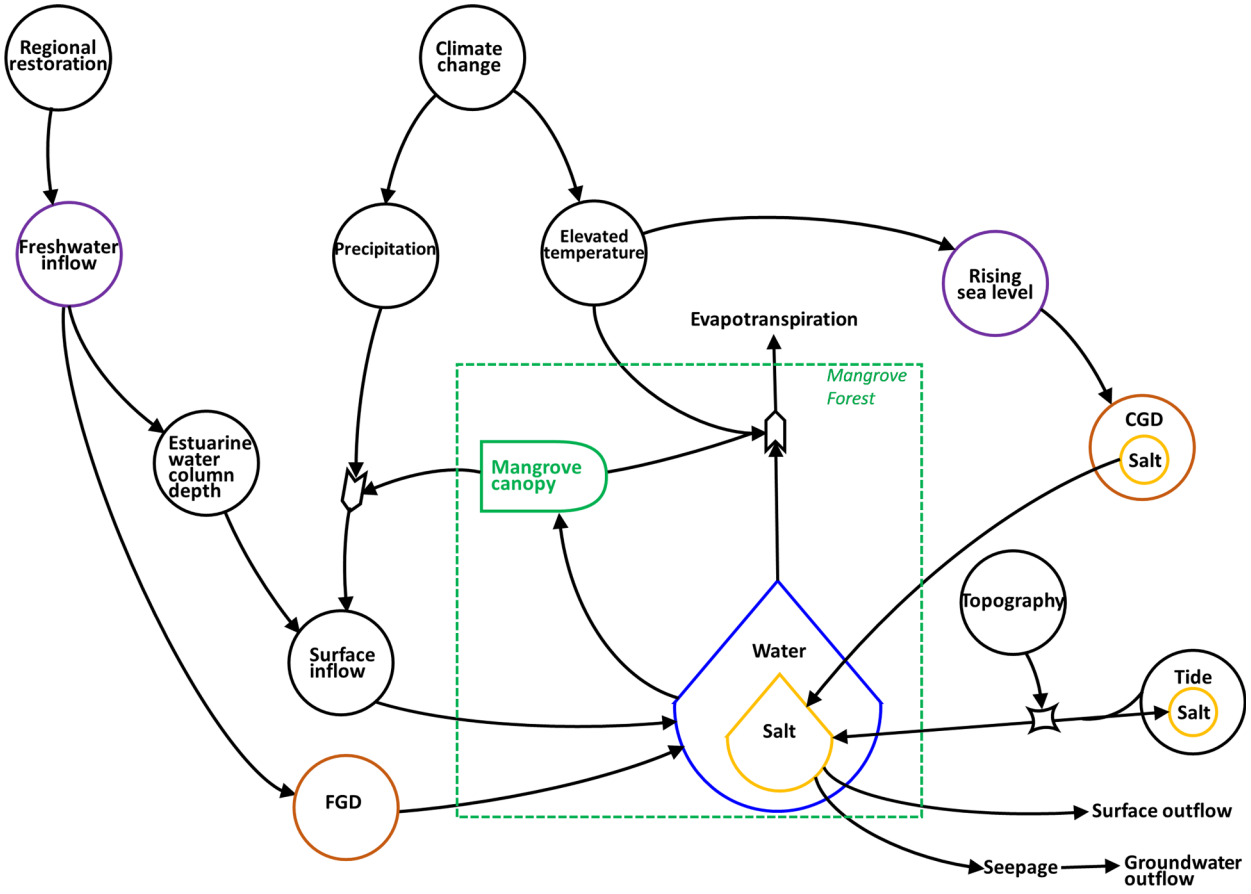

Fig. 2. RHYMAN's mass balance model structure showing drivers, variables and connections. FGD: fresh groundwater discharge; CGD: coastal groundwater discharge (modified from Twilley and Chen 1998). All symbols are from (Odum, 1983).

the water and salt budgets equations implemented in HYMAN (Twilley and Chen, 1998). Thus, changes in water level and salt content in mangrove wetlands can be described using the following water budget equation:

$$\Delta WL/\Delta t = T_i - T_o + P_n + S_i + G_i - ET - S_p \quad (1)$$

where WL is water level (cm) relative to local mangrove soil ground elevation at the end of one unit simulation time ; $\Delta WL/\Delta t$ is water level change per unit time, t (cm day^{-1}); T_i is water flow into the mangrove forest during flood tide (cm day^{-1}); T_o is water flow out of the mangrove forest during ebb tide (cm day^{-1}); P_n is throughfall (cm day^{-1}); S_i is surface sheet inflow (cm day^{-1}), which is defined by a component based on throughfall and is equivalent to runoff; G_i is groundwater inflow (cm day^{-1}); ET is evapotranspiration (cm day^{-1}); S_p is seepage (cm day^{-1}); and salt budget equation:

$$\Delta(S \times WL)/\Delta t = (T_i \times S_t) - (T_o \times S_s) + (G_i \times S_g) - (S_p \times S_{pw}) \quad (2)$$

where S is the porewater salinity at the end of one unit simulation time (g kg^{-1}); $\Delta(S \times WL)/\Delta t$ is the salt content change per unit time, t (g kg^{-1}); S_t is salinity value of the estuarine water during flood tide (g kg^{-1}); S_s is salinity value of flooding water above ground during ebb tide (g kg^{-1}); S_g is groundwater salinity (g kg^{-1}), and S_{pw} is intermediate porewater salinity (g kg^{-1}). The terms $(T_i \times S_t)$ and $(T_o \times S_s)$ represent the salt imported and exported during tidal flooding and ebb tide, respectively; $(G_i \times S_g)$ is the salt imported through groundwater discharge while $(S_p \times S_{pw})$ is the salt lost via seepage; in this context the water level and salt budgets are calculated on a unit area basis.

In this study, the mangrove adjacent estuarine water column is defined as channel water that is influenced by upstream freshwater inflow, tidal exchange, and SLR. The inflow/outflow between the mangrove wetland and the channel combines the relative spatio-temporal dominance of tides and freshwater discharge. We also assume that surface flow is equivalent to surface sheet flow or runoff. Four forcing functions are daily channel water level and salinity, ET, and precipitation registered at or close to each study site (Fig. 1**c-e,** Table 1). Precipitation is considered as the main source of upland water surface flow. Daily seepage is a site-specific constant and represents major outflow along with ET.

RHYMAN explicitly incorporates two groundwater parameters to evaluate daily groundwater inputs (Fig. 2): FGD, the upstream fresh groundwater discharge, a term that considers seasonal freshwater inflow variations, including controlled upstream restoration freshwater diversions; and CGD, the coastal groundwater discharge directly affecting PWS as seawater volume changes due to SLR. Because the impact of both FGD and CGD in the water budget occurs over the long term, these terms are maintained constant during annual simulations in this study. The FGD and CGD values were compiled from published studies or estimated via sensitivity analysis (Table 2). Parameter selection for these components included different values depending on the site location and freshwater inflow volume during the study period. Given the changes in estuarine hydrology during the year, all model simulations for SRS-6 (downstream) and SRS-5 (midstream) sites include CGD seasonal values. In the case of SRS-4, the upstream ecotone site, the FGD was explicitly included to reflect different hydrological conditions in different years, i.e., when freshwater inflow influence was high and sea level was low (Sea Level Anomaly, SLA, range: −2.6 to +1.9 cm; 2004, 2005, 2006, 2008, 2011), while the CGD reflects low freshwater inflow and high sea level (SLA: +4.5 to +8.7 cm) in 2012, 2013 and 2015 (**Table S1**; NOAA, https://www.noaa.gov/; Dessu et al., 2018). We estimated the SLA (**Table S1**) by subtracting the mean sea

Table 1
Data sources and monitoring station locations. Salinity (channel water, soil porewater), hydrology (water level) and climatic variables (precipitation and evapotranspiration) were used for RHYMAN model calibration and validation.

Site	Station ID	Variable	Latitude	Longitude	Source
SRS-6	SRS-6[1]	Water level and PWS[4]	25°21′48.97″N	81° 4′39.34″W	FCE LTER[1]
	SRS-6	Channel water level[4]	25°21′51.91″N	81° 4′41.62″W	FCE LTER
	SRS-6	Channel water salinity	25°21′51.91″N	81° 4′41.62″W	FCE LTER
	SH3[2]	Precipitation	25°21′50.74″N	81° 4′42.53″W	USGS[2]
	SH3	Evapotranspiration	25°21′50.74″N	81° 4′42.53″W	USGS
SRS-5	SRS-5[1]	Water level and PWS	25°22′34.72″N	81° 1′53.67″W	FCE LTER
	SRS-5	Channel water level	25°22′37.28″N	81° 1′56.01″W	FCE LTER
	SRS-5	Channel water salinity	25°22′37.28″N	81° 1′56.01″W	FCE LTER
	Shark River[2]	Precipitation	25°22′29.75″N	81° 2′12.11″W	USGS
	Shark River	Evapotranspiration	25°22′29.75″N	81° 2′12.11″W	USGS
SRS-4	SRS-4[1]	Water level and PWS	25°24′33.13″N	80°57′49.10″W	FCE LTER
	SRS-4	Channel water level	25°24′35.04″N	80°57′51.56″W	FCE LTER
	SRS-4	Channel water salinity	25°24′35.04″N	80°57′51.56″W	FCE LTER
	TE[3]	Precipitation	25°24′29.00″N	80°57′51.00″W	EPN[3]
	TE	Evapotranspiration	25°24′29.00″N	80°57′51.00″W	EPN

[1] Study sites as part of Florida Coastal Everglades Long Term Ecological Research program since 2001 (FCE LTER).
[2] Stations as part of Everglades Depth Estimation Network (EDEN) project maintained by the U.S. Geological Survey (USGS).
[3] Stations maintained by the Everglades National Park (ENP).
[4] Water level = water level inside forest; PWS = porewater salinity; Channel water = the mangrove adjacent estuarine water column.

level (MSL) in 2011 (+3.3 cm) from the MSL values recorded for the rest of the years. Among the study years when freshwater discharge was recorded, MSL value in 2011 is minimum (**Table S1).**

Additionally, nine parameters are site-specific and obtained from most recent field surveys or adapted from HYMAN (Twilley and Chen, 1998). These parameters were classified into two groups: topography and hydrology (**Table 2**). Three topographic parameters (i.e., ground relative surface level, bankfull stage, edge threshold; see definition in **Table 2**) characterize site features given relative elevation settings. Hydrological parameters controlling water and salt exchange are site-specific or adapted from HYMAN, including specific yield for aboveground and underground water, salt content exported by channel water (tidal cycle) or surface flow, and precipitation canopy interception (**Table 2**). Parameterization details are described in **Appendix A**.

The overall RHYMAN structure includes the implementation of four main sub-routines given the study sites stage differences associated with channel and *in situ* water level and local topography (**Fig. S2**). In each sub-routine, water level, salt content, and PWS were calculated sequentially as influenced by each hydrological component during each specific day as included in Eqs. (1) and (2) (**Fig. S2**). The key model results are daily water level and PWS during the simulation period (one year); specific steps to initialize the simulation are described in **Appendix B**. RHYMAN was coded in NetLogo 6.0.4 (http://ccl.northwestern.edu/netlogo), a user-friendly open coding platform (Wilensky, 1999).

2.3. Data acquisition

Hydrological and meteorological data were obtained from long-term monitoring stations (**Fig. 1**, **Table 1**) located along the SRE and maintained by the U.S. Geological Survey (USGS) Everglades Depth Estimation Network (EDEN) project database (https://sofia.usgs.gov/eden/index.php) and FCE LTER database (http://fcelter.fiu.edu). We compiled available daily precipitation and ET data from three EDEN stations (SH3, Shark River, and TE) located close to our study sites (SRS-6, SRS-5, and SRS-4, **Fig. 1b**). Hourly channel water level and discrete channel water salinity (i.e., one sample every three days; see LTER database for details) at each site were compiled on a daily basis. To use the best groundwater discharge and salinity estimation for the FGD parameter, we also compiled data collected at the SH2 station, nearby SRS-4 (**Fig. 1c**), from January 2002 to September 2012 (South Florida Information Access, SOFIA; https://sofia.usgs.gov/).

Sea-level data for the period of 2002–2016 (15 years) were obtained from the NOAA Key West station (**Fig. 1a**; https://www.noaa.gov/). To assess PWS seasonal and spatial variability as a result of local topography, we collected data along a 100-meter transect from the shoreline to the interior of the forest at each site in June (wet season) and November (early dry season) 2018. One topography survey was conducted in December 2017 in all study sites to assess the topographic variation from shoreline towards the interior forest.

2.4. Model calibration and validation

We used the average PWS and daily mean water level registered in the same day from year 2004–2006 to calibrate RHYMAN at each site. PWS was collected in four sampling stations within two 20 × 20 m plots and located near the water level recorder at each site (see study sites section). Calibration parameters include topographic ground surface level, bankfull stage, and hydrological parameters (**Table 2**). RHYMAN was validated using PWS and water level measured from 2007 to 2016. Since channel water level data have large data gaps in some cases, the model was validated using data collected in selected years without or with minor missing data (<10%). The years used for model validations at each site are as follows: SRS-6, 2011, 2012, 2013, 2015, 2016; SRS-5, 2008, 2009, 2011, 2014, 2015, 2016; and SRS-4, 2008, 2011, 2012, 2013 and 2015. The water level data collected during tropical storms/hurricanes (e.g., Hurricane Charley in August 2004 and Hurricane Wilma in October 2005) were excluded and not used for model calibration or validation. All site-specific parameter values for each year are listed in **Table S2**.

2.5. Sensitivity analysis

We conducted a sensitivity analysis to evaluate model performance. We followed the protocol proposed by Jørgensen and Fath (2011) to calculate sensitivity (S) of PWS and water level to the parameter i, where P_i is the best estimated value and ΔP_i represents $a \pm 25\%$ change from the best estimate. Model parameters are summarized in **Table 2** and the equation used for this analysis is listed in **Appendix C.**

2.6. Simulation scenarios

The channel water level and salinity at each station are simultaneously influenced by upstream freshwater discharge and coastal SLR. Given their hydrological importance in regulating PWS, we firstly assessed two potential scenarios using RHYMAN: high freshwater inflow

Table 2
Description, values and units of parameters and drivers used in the mass balance hydrological model RHYMAN.

Group	Parameter	Description	Unit	Magnitude	Source
Topographic	GROUND_SUR	Distance from the local soil ground to the bottom of the control volume	cm	35	this study
	BANKSTAGE	Bankfull stage; Forest maximum standing water depth controlled by local topography during a flooding period	cm	8	this study
	THRESHOLD	Edge threshold; forest flooding criterion determining whether channel water could flood the wetland; this value drives the initial water depth once the wetland is inundated	cm	*site specific*[1]	this study
Hydrological	SY_AB	Aboveground specific yield value	ratio	0.9	Twilley and Chen (1998)
	SU_UN	Belowground specific yield value	ratio	0.065	Twilley and Chen (1998)
	INTERCEPT	Percentage of precipitation that can reach the forest floor i.e. the percentage of rainfall that is not intercepted by the plant canopy	ratio	0.95	Twilley and Chen (1998)
	SALT_EX_TIDE	Mass of salt exported by a gram of tidal water	ratio	0.0003	Twilley and Chen (1998)
	SALT_EX_FW	Salinity dilution ratio by rainfall runoff	ratio	2	Twilley and Chen (1998)
	Legacy_threshold	Salinity criterion that determines whether the salinity legacy procedure is called in cases where salinity is low at the upstream site (SRS-4)	ppt	4	this study
CGD	CGD	Coastal groundwater discharge baseline	cm day^{-1}	1	Smith et al. (2016)
	CGD_Sal	Coastal groundwater salinity	g^{-1}	*site specific*	this study
	times_CGD_incre	Ratio of coastal groundwater discharge to baseline value	ratio	*site specific; yearly*	this study
	%_CGD_dry_to_wet	Coastal groundwater discharge ratio between the wet and dry seasons	ratio	0.5	this study
FGD	FGD	Upstream fresh groundwater discharge baseline	cm day^{-1}	0.4	this study
	FGD_Wet	Ratio of upstream fresh groundwater discharge in the wet season to baseline value	ratio	*site specific*	Saha et al. (2012)
	disperse_FGD	Percentage of salt exported when increasing freshwater recharges the soil subsurface due to dispersion	ratio	0.04	this study
	FGD_Dry	Upland fresh groundwater discharge in the dry season	cm day^{-1}	00	this study
Initial condition	Initial_WL	Initial water level used for water budget calculations at the beginning of each simulation period	cm	*site specific*	this study
	Initial_Salinity	Initial porewater salinity used for water budget calculation at the beginning of simulation period	ppt	*site specific*	this study
Forcing functions	Channel_WL	Depth of water column surrounding mangroves (channel water level) flows into mangroves	cm	*site specific*	FCE LTER
	Sal	Salinity of the water column	ppt	*site specific*	FCE LTER
	ET	Evapotranspiration	cm day^{-1}	*site specific*	FCE LTER
	Precipitation	Precipitation	cm day^{-1}	*site specific*	FCE LTER
Other major hydrological components	Seepage	Amount of subsurface water drained out from the control volume to adjacent channel water per day	cm day^{-1}	*site specific*	this study
	Surface_flow	Water flows out of the control volume through surface flow with assumed 90% runoff coefficient	cm day^{-1}	*site specific; seasonal*	this study
	Sur_Salinity	Salinity of surface flow	cm day^{-1}	*site specific*	this study

[1] Site-specific parameter magnitudes are listed in Table S2.

Table 3
List of scenarios and variable values used in RHYMAN model simulations.

Scenario		Freshwater inflow (mM^3)	Mean sea level (± SE) (cm)	Abnormal sea level (cm)
S0	Baseline	466	3.3 (1.5)	0.0
S1	High freshwater inflow	1562	3.4 (1.2)	0.1
S2	High sea level	440	12.0 (1.3)	8.7
S3	Combination	1412	11.3 (1.4)	8.0

[1]Sea level anomaly is the difference between the mean sea level in specific year and mean sea level in 2011. See Table S1 and model description.

(S1) and high sea level (S2; Table 3). Average freshwater inflow volume along SRS (**Table S1**) under CERP (2001–2016) is approximately 855 Million cubic meters (Mm^3) (Dessu et al., 2018). In 2011, this inflow was below the average volume (466 Mm^3). Meanwhile, SL in the same year was also relatively low (+3.3 cm; SLA: 0). Thus, we selected the channel water level and salinity recorded in 2011 as forcing function values for the control scenario (S0) simulation (*"Channel_WL"* and *"Sal"* in Table 2). In comparison, channel water level and salinity recorded in 2005 were selected as the high freshwater inflow scenario (S1; 1562 Mm^3) with an average "normal" mean sea level (+3.4 cm; SLA: 0.1 cm). Data in the year 2015 were considered as the highest sea level scenario (S2; +12.0 cm; SLA: 8.7 cm) with a "normal" freshwater inflow (440 Mm^3) to investigate - PWS response to higher sea level. To further explore PWS variation under the combined influence of high freshwater discharge and high sea level simultaneously, we defined a combination scenario (S3) using relatively high freshwater inflow (i.e., 1412 Mm^3) and high sea level (+11.3 cm; SLA: 8.0 cm) recorded in 2016 (Table 3). The combination scenario was only conducted for SRS-6 and SRS-5 because field channel water level data had a significant data gap for site SRS-4, hindering the implementation of this scenario. We used precipitation and ET recorded in 2011 (i.e., control scenario; S0) to perform scenarios S1, S2, and S3.

2.7. Statistical analysis

To evaluate model performance, we calculated common statistical measures including model bias, coefficient of determination (R^2), the root mean squared error (RMSE), and the Nash-Sutcliffe efficiency (NSE) (Thomson and Emery, 2014; Wang et al., 2012). NSE values were estimated for each simulation during calibration (2004–2006), validation (2007–2016) procedures, and the full simulation period (2004–2016). Information about these statistical values is included in Appendix D.

We conducted two-way analyses of variance (ANOVA) to determine 1) the differences in field water levels among sites (downstream, midstream, and upstream) and seasons (dry vs wet), 2) the interaction between PWS values across sites and seasons (repeated measures ANOVA), and 3) the interaction between methods (field observations vs modeling simulation) and sites. We also conducted a one-way ANOVA for scenario (S0, S1, S2, S3) simulation results to explore PWS differences impacted by changes in freshwater discharge volume and SLR at each site. The Tukey HSD post hoc comparison ($p < 0.05$) was performed for all ANOVAs. All statistical analyses were performed in JMP Pro 15 (SAS Institute, Cary, NC, USA).

3. Results

3.1. Field measurements: hydroperiod and porewater salinity

Hydroperiod analysis using long term data (2002–2016) showed distinct seasonal and spatial differences along the SRE (**Table S3**). Duration of inundation was higher during the wet season at SRS-6 and SRS-4 compared to the dry season, while slightly higher during the dry season at SRS-5. The difference in seasonal duration was only significant at SRS-4. The frequency of inundation in the dry season was higher than in the wet season across all sites (**Table S3**). Overall, annual flooding duration decreased from downstream to upstream locations along the estuary (SRS-6: 223 ± 6 days yr^{-1}; SRS-5: 206 ± 6 days yr^{-1}; SRS-4: 185 ± 8 days yr^{-1}), while the annual average frequency of inundation was higher at SRS-6 (380 ± 16 events yr^{-1}) that in SRS-4 (214 ± 16 events yr^{-1}) and SRS-5 (176 ± 30 events yr^{-1}).

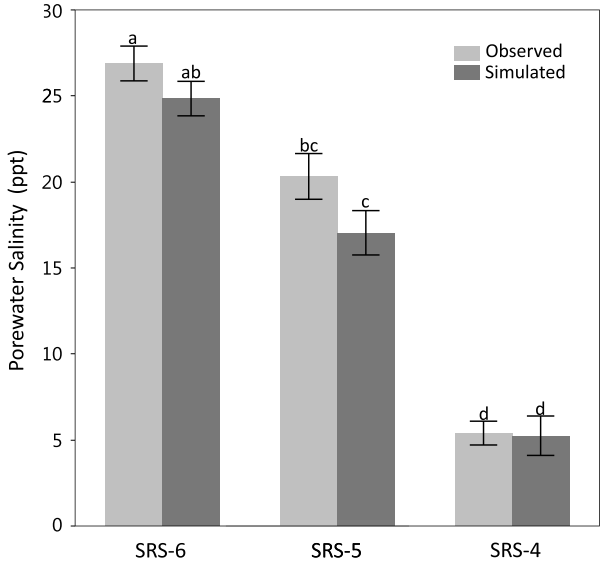

Fig. 3. Comparison between field measurements during the period 2002–2016 (observed) and RHYMAN simulated average soil porewater salinity (PWS) values. Means (± SE) with different letters are significantly different (p-value < 0.05) across sites and method (observed vs simulated).

Mangrove PWS showed significant spatial, interannual and seasonal differences corresponding to seasonal channel water salinity (**Fig. S3, Table S3**). PWS decreased from the downstream (SRS-6) towards the mid- (SRS-5) and upstream (SRS-4) sites and was higher during dry season (**Table S3**). On annual average, PWS was highest at SRS-6 (26.84 ± 1.15 ppt) followed by SRS-5 (20.44 ± 1.51 ppt) and SRS-4 (5.64 ± 0.75 ppt) (Fig. 3).

3.2. Modeling porewater salinity and water level

Simulated annual average PWS was higher at SRS-6 (25.03 ± 0.93 ppt) than in SRS-5 (17.18 ± 1.24 ppt) and SRS-4 (5.27 ± 1.09 ppt), and not significantly different when compared to observed values regardless of sites (MSE = 10.97, $F_{2,2}$ = 0.66, p-value = 0.52; Fig. 3, Table 4). This simulated PWS gradient was consistent with the spatial trend that was observed in the field and reported in other studies (**Fig. S3**) (Castañeda-Moya et al., 2013; He et al., 2020). The average PWS varied among different simulated years for each site (**Fig. S4**), showing distinct interannual and seasonal variation. At SRS-6, the lowest annual average PWS observed in 2005 (22.20 ± 0.40 ppt) was ~8 units lower

Table 4
Summary statistics of annual average soil porewater salinity (PWS) and water level obtained from all calibration and validation simulations.

State variable	Site	Mean	SE	Minimum	Median	Maximum
PWS (ppt)	SRS-6	25.03	0.93	22.20	24.39	30.22
	SRS-5	17.18	1.24	14.08	15.14	24.55
	SRS-4	5.27	1.09	2.57	4.83	12.52
Water Level (cm)	SRS-6	1.36	0.45	−1.11	1.43	3.49
	SRS-5	−6.20	1.38	−14.45	−5.29	0.24
	SRS-4	−7.93	1.95	−14.50	−7.90	1.39

than the highest PWS values in 2015 (30.22 ± 0.18 ppt). The lowest PWS at SRS-5 occurred in 2008 (14.08 ± 0.46 ppt) and the highest in 2015 (24.55 ± 0.31 ppt). In the case of the upstream SRS-4 site, PWS ranged from 2.57 ± 0.16 ppt (2008) to 12.52 ± 0.32 ppt (2015) during the study period. Overall, simulated PWS values throughout the period 2004–2016 showed an increasing trend and peaked in 2015 across all sites while slightly declining by 2016 (**Fig. S4**).

Annual average daily mean water level estimated using RHYMAN decreased from downstream (SRS-6: 1.36 ± 0.45 cm) to midstream (SRS-5: −6.2 ± 1.38 cm), and upstream (SRS-4: −7.93 ± 1.95 cm) (Table 4) reflecting the observed spatial trend in water level along the SRE. Although the simulated water level was a daily value and insufficient to estimate actual inundation duration and frequency inside mangroves, the model replicated seasonal variation inside the forest indicating the general lower water level in the dry season compared to the wet season (**Fig. S5**).

3.3. Model calibration and validation

RHYMAN model simulations during both calibration and validation periods showed good agreement with observed PWS values demonstrating that RHYMAN is capable of simulating PWS dynamics in mangrove forests (Fig. 4, Table 5). For model calibration, simulated PWS values closely matched observed data with a low bias (range: −1.41 to −0.30 ppt) and both high coefficient of determination (R^2; 0.93 to 0.98) and NSE values (0.80 to 0.98) (Table 5). Specifically, the bias was lower at SRS-6 (−0.30 ppt) followed by SRS-4 (−0.50 ppt) and SRS-5 (−1.41 ppt). Coefficients of determination were highest (0.98) at SRS-6 and SRS-5, while the coefficient was relatively lower (0.93) at SRS-4. NSE values estimated for SRS-5 and SRS-6 were the same (0.98) and higher than that of SRS-4 (0.80). Comparatively, the statistical parameters between calibration and validation were different (Table 5). For model validation, the coefficients were higher at SRS-5 (0.88) and SRS-6 (0.74) than in SRS-4 (0.51); whereas NSE values were 0.65 (SRS-6), 0.82 (SRS-5), 0.41 (SRS-4) (Table 5).

Just as in the case during the validation/calibration procedures, simulations for the entire study period (2004–2016) showed good model performance in predicting PWS (Fig. 5,Table 5). Simulated PWS showed low bias (range: −1.96 to −0.86 ppt) and both high coefficients of determination (0.64–0.92) and NSE values (0.56–0.88), indicating that RHYMAN is a robust model to simulate PWS in riverine mangrove forests along the SRE (Table 5). The linear regression between observed and simulated PWS values showed a good agreement at all sites (Fig. 5). A high coefficient of determination was obtained when all paired observed-simulated values were used ($R^2 = 0.94$, RMSE = 2.66 ppt, $F_{1,47} = 749.23$; Fig. 5). RHYMAN is relatively more efficient and powerful when PWS values are estimated for the sites SRS-6 and SRS-5 where seawater and CGD are dominant over upstream freshwater inflow. This was in contrast to the upstream SRS-4 site where the significant composite influence of freshwater inflow and CGD resulted in more complex hydrological patterns.

Although statistical analysis of the simulated water level showed high variability regardless of study periods, simulated patterns captured the spatial trends and seasonal variations in observed daily mean water level inside the forest, which can be attributed to seasonal changes in the adjacent channel water level, ET, and precipitation (Fig. 6, **Fig. S6,** Table 6). Overall, in the case of full period (2004–2016), the simulated water level inside the mangrove forests indicated a slight bias (range: −3.86 to 0.95 cm) and negative/low NSE (−0.28 to 0.02) across all sites; the coefficient of determination at SRS-4 (0.57) was fair, while the coefficients were poor at SRS-5 (0.25) and SRS-6 (0.12) (Table 6).

3.4. Sensitivity analysis

High absolute sensitivity values indicate that water level is sensitive to topographic parameters (i.e., ground surface and bankfull stage;

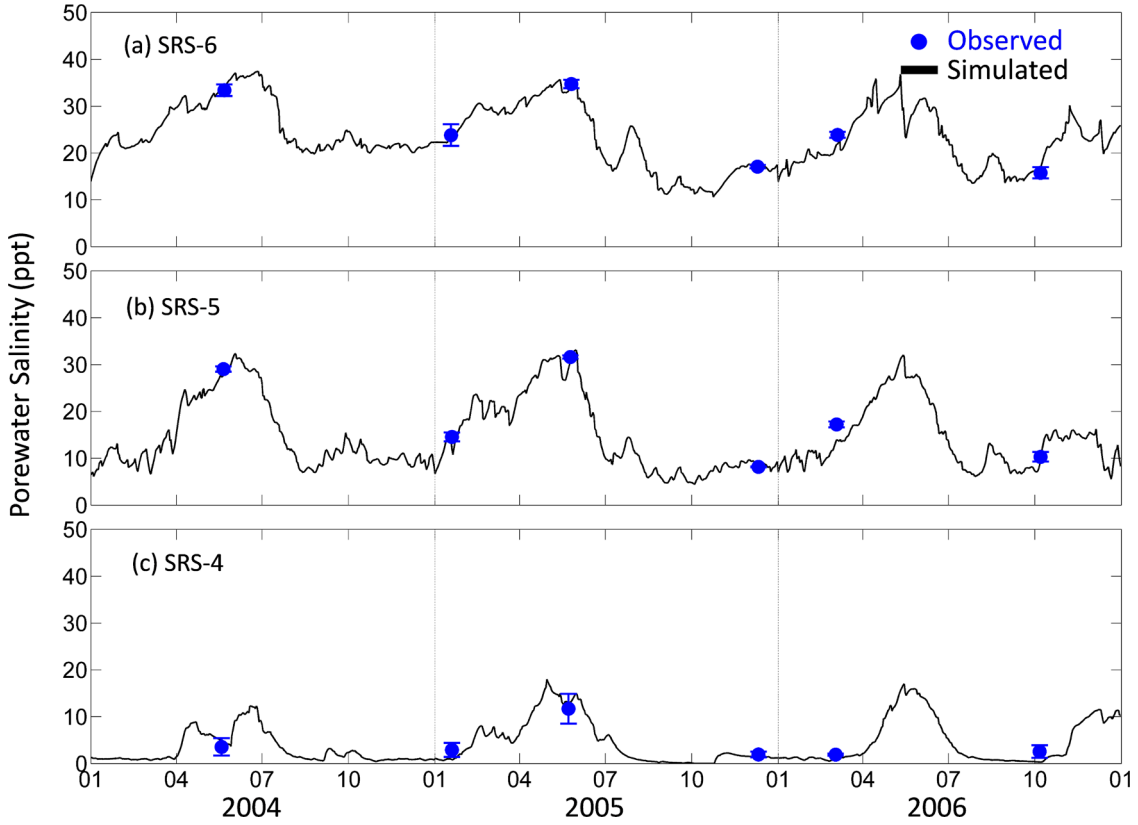

Fig. 4. Soil porewater salinity (PWS) field measurements (observed) inside the mangrove forest in the dry and wet seasons (2004–2006); continuous line (simulated) shows RHYMAN model calibration results.

Table 5
Soil porewater salinity (PWS) statistical information estimated for the partial (i.e., calibration: 2004–2006; validation: 2007–2016) and full (2004–2016) simulation periods (see methods for details).

Period	Site	# of Sample	Bias[1] (ppt)	Mean (ppt)		R^2 (1)	RMSE[1] (ppt)	NSE[1]
				Observation	Simulation			
Calibration (2004–2006)	SRS-6	6	−0.30	24.78	24.48	0.98	1.18	0.98
	SRS-5	6	−1.41	18.48	17.07	0.98	1.45	0.96
	SRS-4	6	−0.50	4.10	3.60	0.93	1.41	0.80
Validation (2007–2016)	SRS-6	10	−1.72	26.30	24.58	0.74	3.42	0.65
	SRS-5	11	−2.27	23.70	21.44	0.88	3.12	0.82
	SRS-4	10	−1.07	6.73	5.66	0.51	3.11	0.41
Full (2004–2016)	SRS-6	16	−1.19	25.73	24.54	0.84	2.80	0.80
	SRS-5	17	−1.96	21.86	19.89	0.92	2.58	0.88
	SRS-4	16	−0.86	5.74	4.89	0.64	2.75	0.56

[1] For definitions and calculations see Appendix D.

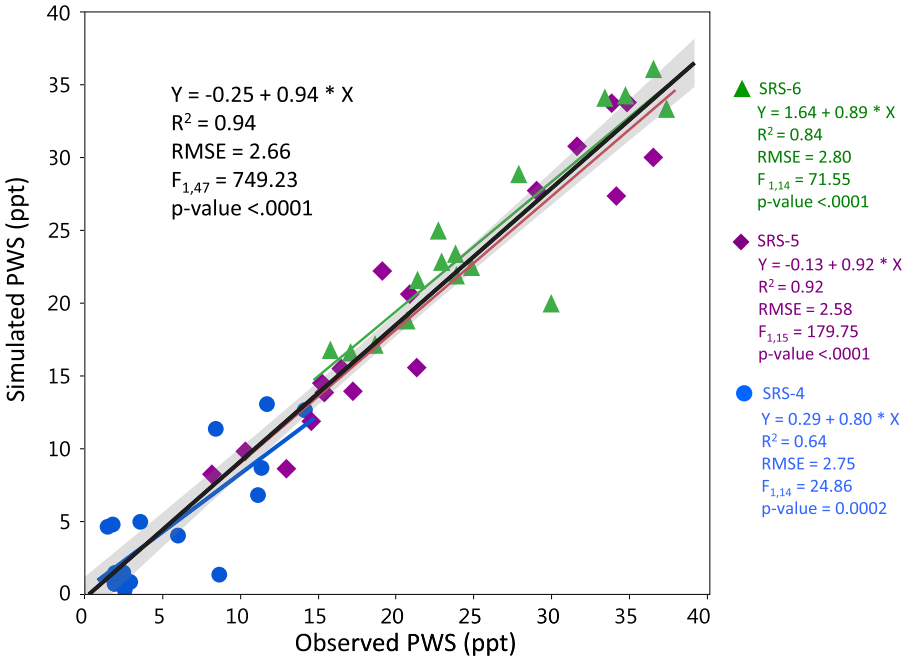

Fig. 5. Linear regressions between soil porewater salinity (PWS) field measurements and RHYMAN model simulation results at each study site along the Shark River estuary. Field measurements were obtained in the period from 2004 to 2016 in the dry and wet seasons (see methods). Light gray area indicates the 95% confidence interval for the full model (black line).

Table 7) given the integrative role that local topography plays in controlling hydroperiod inside the mangrove wetlands. In contrast, PWS was not sensitive to any parameter with a ± 25% change which indicates that changes in PWS were less than 25% in these cases. PWS sensitivity values were generally smaller (|S| <0.10) across all sites. The CGD procedure showed that the sensitivity to the parameter (i.e., CGD differences between dry vs wet seasons; %%CGD_dry_to_wet, Table 2) is relatively higher at SRS-5 (S = 0.13). The sensitivity value of dispersion in the FGD procedure (dispersion_FGD) was −0.2, underscoring its larger influence on model performance than other model parameters (Table 2).

3.5. Simulation scenarios

The PWS values were significantly different among the four simulation scenarios across sites (Fig. 7, **Table S4**). The control scenario (S0) showed a similar gradient of annual average PWS values across sites compared to field measurements where the higher salinity was registered at the downstream and midstream estuary (SRS-6: 27.18 ± 0.32 ppt; SRS-5: 21.04 ± 0.41 ppt) and the lowest values at the upstream site (SRS-4: 4.96 ± 0.27 ppt). In the case of the high freshwater discharge scenario (S1), when compared to S0 results, PWS was significantly reduced by 4.50 and 5.64 ppt units at SRS-6 and SRS-5 respectively, while at SRS-4 remained approximately the same in both scenarios S0 and S1 (4.61 ± 0.25 ppt). PWS values were high in the high sea level scenario (S2) with a significant increase in PWS values regardless of site locations; the maximum PWS increase was at SRS-4 (7.61 ppt), followed by SRS-5 (3.54 ppt) and SRS-6 (3.02 ppt). The mean PWS simulated at SRS-6 under this combined scenario was significantly lower than the values obtained in the control scenario (i.e., 24.01 ± 0.19 ppt). In the case of SRS-5, the average simulated PWS was 15.39 ± 0.21 ppt under S3, which is approximately same as S1 (15.39 ± 0.46 ppt), but significantly lower compared to S0 (21.04 ± 0.41) and S2 (24.57 ± 0.33) scenarios (Fig. 7, **Table S4**).

4. Discussion

4.1. Model performance

Simulated PWS values along the SRE using RHYMAN showed close agreement with historical field measurements (Fig. 5), indicating that this mass balance-based modeling approach has strong utility in

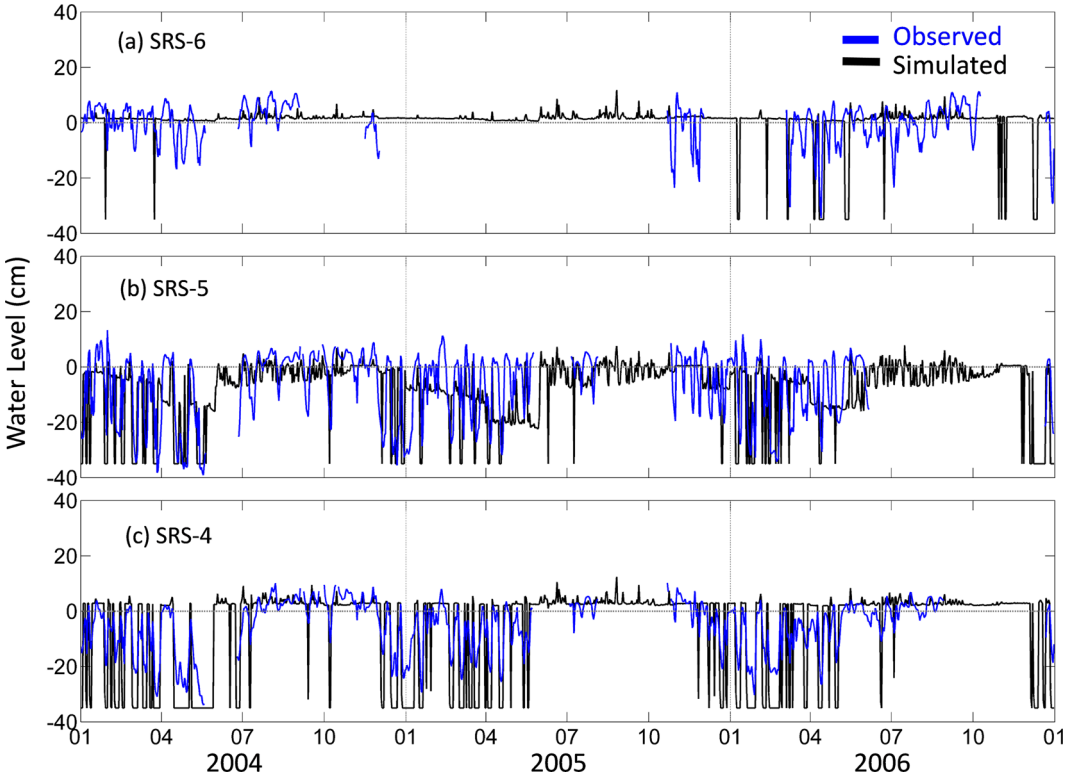

Fig. 6. Field measurements (observed) and RHYMAN modeling (simulated) daily water levels inside the mangrove forests.

forecasting PWS in riverine mangrove forests under different hydrological scenarios. Model performance in this study was improved when compared to a previous PWS modeling estimation along the SRE over the period of 2003–2005 using HYMAN without explicitly considering groundwater inputs (FGD and CGD) (i.e., Tsai, 2008). For instance, Tsai (2008) showed that simulated PWS values at SRS-4 during the wet season were ~5–7 ppt greater than the observed PWS range. This result was attributed to salt accumulation in the soil due to low precipitation and high ET in late spring and then flushed out in the summer season. However, when we included the term FGD, the simulated PWS matched the field observations in the period of 2004–2005. One mechanism explaining this temporal agreement is that increasing upstream freshwater inflow causes a reduction in salinity concentration in both the adjacent channel water and groundwater at SRS-4 (Lagomasino et al., 2015); thus, the combination of fresher channel water and groundwater inputs decreases PWS inside the mangrove forest. Simultaneously, excess freshwater inputs into the soil matrix might also help export or disperse more salt to adjacent estuarine waters through surface flow and seepage. The relatively high absolute sensitivity value of dispersion (0.2) indicates the considerable influence of salt dispersion on PWS.

Similar to the functional role of the term FGD at upstream estuary locations, the inclusion of the parameters defining CGD also improved PWS projections in both SRS-5 and SRS-6 sites when compared to previous estimates (i.e., years 2004 and 2005; Tsai, 2008). The region close to the estuary mouth (e.g., downstream SRS-6) is characterized by a thick peat layer (~3–6 m; Whelan, 2005; Yao and Liu, 2015; 2017). Consequently, the local aquifers are relatively deep in downstream SRS-6. The relative contributions of groundwater stored in the deep aquifers has a limited effect on net water volume and salinity in the subsurface. Instead, CGD is associated with seawater/brackish water intrusion into the mangrove soil, as shown by isotope markers in the SRE, and can potentially alter PWS (Price et al., 2003; 2006; Smith et al., 2016). In RHYMAN, CGD represents the subsurface/shallow water flow (< 1 m) discharge into the mangrove soil; therefore, the relatively high

Table 6
Water level statistical information estimated for the partial (i.e., calibration: 2004–2006; validation: 2007–2016) and full (2004–2016) simulation periods (see methods for details).

Period	Site	# of Sample	Bias[1] (cm)	Mean (cm)		R^2 (1)	RMSE[1] (cm)	NSE[1]
				Observation	Simulation			
Calibration (2004–2006)	SRS-6	575	0.47	0.26	0.73	0.04	6.41	−0.39
	SRS-5	780	−3.35	−6.29	−9.64	0.18	10.86	−0.18
	SRS-4	932	−3.24	−3.28	−6.52	0.65	9.69	−0.08
Validation (2007–2016)	SRS-6	1335	1.16	0.51	1.68	0.16	5.10	0.13
	SRS-5	1416	−1.05	−3.47	−4.52	0.28	9.70	0.15
	SRS-4	1295	−4.30	−3.04	−7.33	0.53	11.83	−0.40
Full (2004–2016)	SRS-6	1910	0.95	0.44	1.39	0.12	5.54	0.02
	SRS-5	2196	−1.87	−4.47	−6.34	0.25	10.29	0.05
	SRS-4	2227	−3.86	−3.14	−6.99	0.57	11.01	−0.28

[1] For definitions and calculations see Appendix D.

Table 7
Sensitivity analysis (± 25% level) of different parameters for ground surface (GROUND SUR), bank stage (BANKSTAGE), aboveground specific yield (SY_AB), belowground specific yield (SY_UN), salt tidal exchange (SALT_EX_TIDE), forest canopy precipitation interception (INTERCEP), coastal groundwater discharge (CGD), seasonal CGD percentage (%%CGD_dry_to_wet), salt dispersion (dispersion_FGD), and fresh groundwater discharge (FGD).

		Parameter[1]									
State variable	Site	GROUND SUR	BANK-STAGE	SY_AB	SY_UN	SALT_ EX_TIDE	INTER-CEPT	%CGD_ dry_to_wet[2]	CGD[2]	Dispersion _FGD[3]	FGD[3]
PWS (ppt)	SRS-6	0.01	0.00	−0.05	−0.07	0.01	−0.06	0.07	0.02	nd[2]	nd[2]
	SRS-5	0.00	0.05	−0.03	0.00	0.00	−0.06	0.13	0.05	nd[2]	nd[2]
	SRS-4	0.00	0.00	0.08	0.03	−0.03	−0.10	nd[3]	nd[3]	−0.20	0.01
Water Level (cm)	SRS-6	−0.03	59.47	111.16	64.71	0.20	1.04	2.92	0.91	nd[2]	nd[2]
	SRS-5	−0.12	−5.69	−9.94	−5.99	−0.40	−0.07	−0.79	−0.32	nd[2]	nd[2]
	SRS-4	−0.21	−1.20	−0.93	−0.94	−0.18	−0.05	nd[3]	nd[3]	0.00	−0.03

[1] See Table 2 for parameter description.
[2] No data for the variables related to CGD parameters at SRS-6 and SRS-5. See model description section.
[3] No data for the variables related to FGD parameters at SRS-4. See model description section.

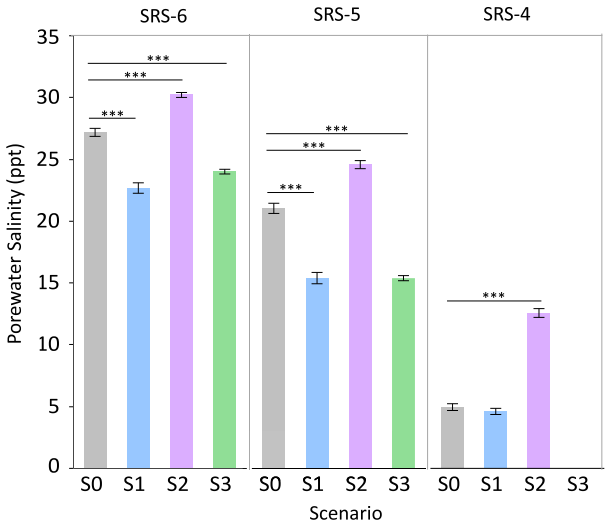

Fig. 7. Means (± SE) soil porewater salinity (PWS) values from four RHYMAN simulation scenarios at each site. Scenarios are S0: Baseline; S1: High freshwater inflow; S2: High sea level; and S3: Combination. *** indicates significant difference from the baseline scenario (S0) at each site.

agreement between observed and simulated PWS values at SRS-6 and SRS-5 indicates that the CGD would increase PWS values as saline water slowly enters the subsurface soil as a result of seawater intrusion driven by sea-level rise over the long term (Fig. 5). In contrast, as the peat soil layer (~1.5 m depth) becomes shallower upstream (SRS-4), groundwater input (i.e., freshwater; FGD) from the deep aquifer becomes significant (Smith et al., 2016), especially in the context of freshwater diversions as part of the hydrological restoration program upstream the ENP (National Academies of Sciences, 2016; Sklar et al., 2005; Troxler et al., 2013). However, even after including the FGD parameters, the interaction between fresh and brackish groundwater sources is still complex at SRS-4 leading to relatively poor PWS simulation compared to the SRS-6 and SRS-5 sites (Fig. 5, Table 5).

Simulated PWS in riverine mangrove forests along SRE captured the spatial variation in field measurements with high values in SRS-6 and SRS-5 and low values in SRS-4 during both wet and dry seasons (**Fig. S3, Table S3**). The apparent PWS decreasing trend from downstream SRS-6 towards mid- and upstream (SRS-5 and SRS-4) reflects hydrological processes and their interactions at the regional scale; particularly at the two endmember sites, downstream (SRS-6) and upstream (SRS-4; **Fig. S5, Table S3**). The EMER is delimited by the Gulf of Mexico coastline and comprises an extensive hydrological network with multiple interconnected estuaries/tidal channels (Castañeda-Moya et al., 2020; Rivera-Monroy et al., 2011). For example, the site SRS-4 is located upstream in Tarpon Bay, at the junction between the Shark and Harney Rivers (Fig. 1**c**). Longer inundation duration in wet season based on field measurements at SRS-4, compared to midstream SRS-5, shows that water level upstream is influenced by the Shark and Harney Rivers (**Table S3**). Although the hydrological interaction between these two rivers remains uncertain, the compounded hydrological synergy does modulate water budgets and materials exchange in this area, as observed by distinct sedimentation patterns during natural disturbances and associated storm surges (Castañeda-Moya et al., 2020). Further, this complex hydrological coupling is also evident by the opposite trend in flooding duration at SRS-5 (longer in the dry season) in comparison with SRS-6 and SRS-4 (longer in the wet season). In the wet season, the relatively high river discharge upstream can potentially offset the downstream tidal flooding regime. Hence, this offset across sites, along with seasonal ET and precipitation (**Fig. S6**), may explain the lower duration of inundation at the midstream site (SRS-5) during the wet season. This long-term offset, captured by RHYMAN simulations, highlights the dynamic hydrological interaction between river discharge and tides at the SRS-5 location, which is part of a complex network of channels and tidal creeks (Fig. 1**a**) (Larsen et al., 2012; Nuttle et al., 2000). In contrast to SRS-5 and SRS-4, SRS-6 hydrological conditions are dominated by strong tidal dynamics due to its proximity to the Gulf of Mexico (Fig. 1**e**) that results in higher inundation frequency and water level inside the forest. Although RHYMAN does not explicitly include functions representing tidal asymmetries and material exchange (water and salt) through water movements between the forest and the water column at the mouth of the estuary (e.g., Mazda et al., 1995; van Maanen et al., 2015; Wu et al., 2001), our mass balance approach implicitly capture their effect on PWS seasonal variability.

Seasonal variations in simulated PWS values were consistent with observations and previous studies (**Fig. S4, Table S3**) (Castañeda-Moya et al., 2013; Chen and Twilley, 1999) and highlights the critical role of hydroperiod in regulating PWS in mangrove forests (Krauss et al., 2006; Lara and Cohen, 2006). For instance, although the frequency of inundation is higher during the dry season in SRS-4, the average low water depth and shorter inundation duration reduce the interaction between subsurface porewater and surface water during flooding. This limited interaction reduces salt exchange between the forest and adjacent estuarine water. The high frequency of inundation during the dry season was a composite result of relatively low water depth and shorter flooding duration, which underscores the complex attributes of hydroperiod (**Fig. S5**) (Friess and Watson, 2016; Rivera-Monroy et al., 2017). Additionally, seepage is low due to the low crab burrow density in this site (Smith et al., 2016), thus accumulating a greater proportion of salt. This composite interaction among variables results in the seasonal salinity or “salt legacy”, which largely influences simulated PWS values, as RHYMAN simulations showed in SRS-4

during the dry season (e.g., Castañeda-Moya et al., 2006; Krauss et al., 2006). This inclusion of salt legacy considers its influence from the previous time step (i.e., day) when calculating the PWS in a current simulation day, thus improving the agreement between simulated PWS and field measurements (Tsai, 2008). This improvement underscores the relative importance of "salt legacy" in regulating salt balance in the long term, especially in cases where mangrove soil is influenced by varying flooding regimes and hydroperiod gradients, as in the case of areas with low-level topography (i.e., Taylor River Slough, Everglades) and semi-arid coastal regions characterized by micro-tides (< 30 cm) (Sánchez-Carrillo et al. 2009).

Conversely, in areas where crab burrow density is high, the soil is less saturated as a result of greater flushing of materials, including salt, during the dry season. This is the case of site SRS-6 where burrows are efficiently flushed (up to 100% efficiency) due to tidal pumping during the dry season (Smith et al., 2016). This mechanism partially explains why our simulated PWS values are close to field measurements, since the influence of "salt legacy" at SRS-6 in the long term is low compared to SRS-4. Thus, the water exchange interacting with soil properties (e.g., bulk density, crab burrows presence) at different temporal scales (i.e., tidal and seasonal forcing) is critical in regulating not only salt exchange, but also nutrient availability (i.e., soil TP and soluble reactive phosphorus- PO_4^{-3}) and carbon storage in the long term (Santos et al., 2019; Tait et al., 2016; 2017). Further studies are needed to quantify this net water exchange in mangrove ecosystems under different geomorphic settings and hydroperiod regimes, especially in wetlands influenced by microtidal regimes (Kristensen et al., 2017; Smith et al., 2016).

4.2. Considerations concerning RHYMAN model settings and boundaries

As a spatially implicit model, RHYMAN was designed and calibrated using the water level relative to the forest soil surface as a criterion to assess flooding events during tidal exchange. To reflect the local topography influence, the bankfull stage was explicitly included in the model (**Fig. 2**). The high sensitivity values of the topographic parameters highlight the importance of capturing the forest elevation gradient when simulating water level in our mangrove sites where topographic relief is significantly different along the estuary (**Table 2**).The inclusion, for instance, of the bankfull stage is critical to adjust the local water level affected by local topographic gradients. Indeed, the observed PWS values sampled along a 100-meter transect at each site (**Fig. S1**) slightly decreased from the channel bank (i.e., the water edge where the channel water level recorder was installed) to the forest interior. These spatial differences in PWS values along the topographical gradient is the outcome of a highly dynamic vertical exchange of water and salt between the soil and the overlying water during flooding conditions at different temporal scales (tidal vs seasonal). In this case, the simulated PWS is assumed as the averaged value due to water flows across soil layers with different soil properties (e.g., porosity) in our mass balance approach. This is one of the reasons why our water level simulation results are different from direct measurements. Overall, the sensitivity analysis showed a robust model performance regarding topography as a controlling variable where PWS values were not very sensitive (i.e., ± 25%) to the ground surface level and bankfull stage parameters (**Table 7**). Nevertheless, it is important to carefully select these parameters during the calibration and validation stage in other environmental settings and mangrove ecotypes (e.g., scrub, basin), especially when using RHYMAN to evaluate PWS at larger spatial scales. This step is critical given that the edge threshold is a site-specific parameter obtained using regression analysis (Tsai, 2008). Specifically, the topography inside forests and channel bathymetry are dynamic over a long term due to sediment transport, deposition and accumulation associated with tidal exchange or hurricane events (Castañeda-Moya et al., 2020; Feher et al., 2019).

RHYMAN defines a boundary condition by using a constant ground surface level (Twilley and Chen, 1998). This selection is based on the initial assumption that, when the adjacent channel water flows into the forest, there is surface water flow that then recharges and maintains a subsurface water level which becomes the boundary condition. Given the long-term field PWS data availability at 30-cm depth in our study sites, it was adequate to use the ground surface level boundary at 35 cm. Our model does not explicitly include the channel water column lateral pressure. This lateral pressure, as related to Darcy's law (Mazda and Ikeda, 2006), still can influence groundwater level through subsurface flow, especially in cases where soil porosity is high due to crab burrows, as is the case in our study sites (Larsen et al., 2011; Smith et al., 2016). Although we considered seepage outflow, which contains the partial influence of lateral pressure, the performance of RHYMAN model was limited when simulating water level inside the forest. The observed lowest water level was approximately 20–40 cm belowground, indicating that the boundary water level is maintained probably belowground within this range (**Fig. 6**). To improve water level simulations inside the forest, further field surveys are needed to evaluate this key boundary value currently included in RHYMAN.

We also attribute the difference between observed and simulated water level values, as indicated by the negative NSE value, to the fact that RHYMAN simulates a daily water budget. Using forcing variables on a daily basis as a simplified approach does not consider the dynamic processes regulating water and salt exchange within a semi-diurnal tidal cycle (**Table 2;** Eqs. (1) and (2)). This daily step limits the evaluation of water and salt budgets through each tidal cycle (~12-hour period) as implicitly considered in the mass balance calculations at each location affected by semi-diurnal tides. Further, by omitting explicit hydrodynamic processes, our model is not able to examine water flow inside the forests and its interactions with the soil surface and trees/roots (i.e., shear stress or drag force) (Mazda et al., 2005). Hence, the model cannot estimate how the energy dissipates as water flows in/out of the forest and its concomitant impact on water and salt budgets (Larsen and Harvey, 2010; Mazda et al., 2005); especially considering the high drag force caused by highly dense prop roots (Alongi, 2009; Castañeda-Moya et al., 2011; Lugo and Snedaker, 1974; McKee et al., 1988; Tomlinson, 2016; Troxler et al., 2015). As a result, PWS can be over/underestimated (range: ~1–10%) depending on the season and the relative effect of FDG and CDG procedures in the overall salt and water budget simulations (**Fig. 5**). Despite this limitation, RHYMAN's PWS values are robust estimates when using a mass balance methodology as is the case for other studies in coastal ecosystems including salt marshes and tidal freshwater forested wetlands (Morris, 1995; Wang et al., 2007; Wang et al., 2020).

Furthermore, our results show the model potential to be expanded into a spatially explicit setting to evaluate the contribution of PWS as a stressor in modulating forest structure, aboveground biomass, and NPP trends. Thus, RHYMAN offers an experimental opportunity to evaluate future changes in mangrove wetland spatial distribution and NPP in the long term (annual, decadal) as climate changes in coastal Everglades (Flower et al., 2019; Saha et al., 2012; 2011). Similarly, given the computational expense, it is an inefficient strategy to simulate hourly PWS fluctuations as expected in a more complex hydrodynamic model. Overall, this type of models requires further parameterization that limit their utilization, especially given the lack of field data in most mangrove forests at tropical latitudes (e.g., Rivera-Monroy et al., 2004).

4.3. Porewater salinity dynamics under increasing freshwater restoration and rising sea level

The Shark River Slough is one of the main drainages delivering groundwater and surface freshwater from upstream Everglades into the SRE and directly impacting our study sites (**Fig. 1**). In our scenario simulations (**Table 3**), the high freshwater inflow scenario (S1; 1562 Mm^3) has 3.5 times freshwater discharge than the control scenario (S0; 446 Mm^3) and causes a decrease in PWS values at SRS-6 (17%) and

SRS-5 (27%), while maintaining PWS values at SRS-4 (~4–5 ppt). As expected, this decreasing spatial trend in PWS values indicates a reverse relationship between freshwater inflow and PWS values. A similar response to freshwater increase has been reported in other South Florida regions. For example, modeling results (March 2007-October 2009) showed a reduction from 18 to 10 ppt in groundwater/subsurface salinity in the brackish/saline marsh-mangrove ecotone at the Ten Thousand Island National Wildlife Refuge (Michot et al., 2017); this reduction was related to a potential increase in 20% freshwater inflow under CERP management decisions. Yet, a recent field study in the same region found that an actual reduction in freshwater discharge compounded by increasing SLR has caused salt intrusion and an increase in overlying water in flooded freshwater marshes (Romañach et al., 2019). Together, these results show the relative rapid Everglades regional ecosystem response to both freshwater diversions and SLR. This response is most probably due to the karstic porous geomorphic setting with low topographic relief, high hydraulic conductivity, and close coupling between surface water and groundwater processes (Dessu et al., 2018; Price et al., 2006; Saha et al., 2012; Smith et al., 2016).

In contrast, when saltwater enters the SRE due to increasing SL, salinity increases commensurably with saltwater inputs from the Gulf of Mexico. This is the case under a high sea level scenario (S2) with PWS increasing about 11% at SRS-6, 17% at SRS-5, and by 1.5 times upstream at SRS-4 when compared with the control scenario (S0; **Fig. 7, Table S4**). Indeed, this scenario (S2) will become the "new normal" due to the rapid increasing SLR in this region over the last decade (9 ± 4 mm yr^{-1}; three times of average pre-2006 rate, 3 ± 2 mm yr^{-1}) (Wdowinski et al., 2016), and similar to other coastal regions in the United States where SLR is accelerating (**Table S1;**Dahl et al., 2017). An increase in PWS up to 40 ppt will not impact mangrove functioning and extent overall since these coastal wetlands are adapted to withstand PWS up to >70 ppt depending on hydroperiod (Lugo and Medina, 2014); especially flooding duration and frequency (e.g., Castañeda-Moya et al., 2006). However, as PWS increases, we expect a significant expansion in mangrove area with the species *R. mangle, L. racemosa,* and *C. erectus* readily occupying marsh habitats close to the upstream boundary (SRS-4). This is because the PWS along the boundary is more sensitive to increasing sea level as the S2 simulation showed. The expansion pattern has been observed in the Ten Thousand Islands region of southwestern Florida (Howard et al., 2017; 2020) and Taylor River Slough, where there is a distinct boundary defined by a mix of mangrove-marsh vegetation ("white zone"; Ross et al., 2000) that has moved inland since the 1940s. This area has a net area gain, as dry conditions are triggered by a reduction in freshwater delivery as a result of past CERP management (National Academies of Sciences, 2016) interacting with "dry", low precipitation years triggered by the ENSO (Davey et al., 2014).

Further, a current long-term landscape-level assessment (1985–2017) shows a cumulative increase (+10.2%) in mangrove coverage in the FCE (Han et al., 2018). This transgression/encroachment has been common in this coastal region since the early-mid Holocene epoch when mangrove wetlands colonized downstream areas of SRE around 3800 cal yr BP by encroaching into the freshwater marsh as sea-level rose (Yao and Liu, 2015; 2017). For instance, similar vegetation habitat shifts from coastal marsh (i.e., freshwater, brackish and saline) to scrub mangroves (e.g., *A. germinans*) have been associated with increasing SLR and air temperature along the Louisiana and Texas coastal regions in the northern Gulf of Mexico (Guo et al., 2017; McKee and Vervaeke, 2018; Osland et al., 2013; Saintilan et al., 2014). Although there is mangrove expansion in the EMER (Han et al., 2018), roads, channels, and other infrastructure features will eventually cause a "coastal squeeze" (Enwright et al., 2016) where limited space will stop this vegetation expansion.

A comprehensive PWS spatiotemporal assessment along the SRE requires consideration of the combined effects of freshwater inflow, sea level, and climatic factors. In particular, long-term (2001–2016) water column salinity changes were more evident as a result of changes in freshwater inflow and sea-level rise than from interannual variation in ET and precipitation, despite their covariation with elevated global temperature (Dessu et al., 2018). This outcome was observed in the RHYMAN combination scenario (S3; **Fig. 7,Table S4**) at SRS-6 site where, despite an increase of 6% in PWS compared to S1, PWS did decrease 20% in contrast with the value under S2. Certainly, this result suggests that high freshwater inflow can offset the relative impact of high SL on PWS values. In fact, Dessu et al. (2018) pointed out that freshwater inflow and water level above the SRS-4 site were critical variables in maintaining a "fresh-to-marine head difference", which they considered the critical factor affecting marine-to-fresh water connectivity and transport of salinity and nutrients along the SRE.

Overall, if reducing mangrove expansion into freshwater/brackish marshes is one of the CERP management priorities, then increasing freshwater inflow is needed as suggested by RHYMAN scenario simulation (S2 vs. S3). On the contrary, freshwater reduction and SLR, resulting in PWS increase, can facilitate mangrove survival and expansion landward, thus increasing mangrove area (S2) (Han et al., 2018). Specifically, our modeling results show that during a tropical storm (e.g. Hurricane Wilma, October 2005; **Fig. 5**) PWS can rapidly increase at upstream SRS-4, despite high precipitation induced by the storm, suggesting the dominant role of seawater intrusion associated with major storm surges (Castañeda-Moya et al., 2020; Lagomasino et al., 2020; McKee et al., 2016). This instantaneous increase also reiterates that the PWS at the boundary site SRS-4 is sensitive to the seawater intrusion. Thus, the RHYMAN S3 simulation results highlight complex interactions among the hydrological components and the major impact of SLR on water and salt exchange, especially along the mangrove-marsh ecotone boundary (SRS-4).

4.4. Mangrove forest structure and salinity gradients

PWS and hydroperiod in the SRE, along with well-documented differences in soil total phosphorus (TP) concentrations regulated by hurricanes (Castañeda-Moya et al., 2020; Danielson et al., 2017), are key factors controlling mangrove species composition, tree height, and NPP patterns (Castañeda-Moya et al., 2013; Chen and Twilley, 1999; Danielson et al., 2017; Lagomasino et al., 2020; Rivera-Monroy et al., 2019; Smith et al., 2009). But the lower PWS values at SRS-4 (~1–14 ppt; **Table S3**), for instance, allows the presence of freshwater/brackish vegetation and the exclusion of the mangrove species *A. germinans* (Danielson et al., 2017). This species, present at SRS-5 and SRS-6, is physiologically more tolerant to higher salinities where tree growth rate and density increase even in seasonally hypersaline conditions (e.g., arid zones in the Caribbean and Pacific regions, Castañeda-Moya et al., 2006; Ochoa-Gómez et al., 2018) that are currently absent in the SRE. Indeed, during the last 6 years freshwater/brackish vegetation has expanded at SRS-4 as PWS remained low during this period (<10 ppt). This vegetation is now competing with mangrove species for space and other resources (e.g., nutrients and light) resulting in the replacement of dominant mangrove species (i.e., *R. mangle*, 61%) by other brackish tree species like *Chrysobalanus icaco* (coco plum), which is also found in tree islands upstream in the Everglades (van der Valk et al., 2008). Thus, if freshwater flow increases as part of the CERP restoration plans, it is expected that as the salinity regime changes along the SRE, the relative dominance and extension of mangrove forests might also change at the boundary between freshwater/brackish and saline gradients (Danielson et al., 2017; Dessu et al., 2018; Michot et al., 2017).

Past and current hydrological assessments have proposed that the EMER might be already in a transient state, probably far from the pre-development hydrological conditions of the 1950s (Dessu et al., 2018; Rivera-Monroy et al., 2019). Thus, there is a need for a comprehensive assessment of the initial criteria to decide on the quantity, quality,

timing and distribution of freshwater (Sklar et al., 2005) along the Shark River Slough and other locations throughout the southern Everglades, including the SRE (Flower et al., 2017). If one of the CERP goals is to re-establish freshwater vegetation, then any increase towards pre-development hydrologic conditions will result in slowing mangrove expansion into freshwater marshes due to salt intrusion (S3), but it may also alter species diversity at the upstream boundary. Management decisions are especially needed given the potential economic impacts in the case of mangrove wetlands spatial distribution. Further studies are needed to evaluate these potential vegetation spatiotemporal distribution outcomes based on a contemporary evaluation of desirable ecosystem services such as carbon sequestration (e.g., blue carbon in mangroves; Jerath et al., 2016) and habitat biodiversity associated to low PWS (e.g., *Cladium jamaicense*-dominated seagrass) in the Everglades landscape.

5. Conclusion

A mass balance-based hydrological mangrove model—RHYMAN—was developed and implemented for riverine mangrove forests in the SRE that explicitly considers groundwater discharge associated with upstream freshwater input (FGD) and coastal groundwater discharge (CGD). RHYMAN simulated water and salt budgets at three sites along the estuary and matched observed daily and seasonal soil porewater salinity (PWS) associated with spatial differences. Although RHYMAN's daily water level simulations were constrained and variable, the model was able to evaluate the relative regulatory role and effect of freshwater inflow and SLR on PWS. Modeling results show that lower freshwater inflow volume and higher SLR lead to higher PWS values in mangrove forests along the SRE. Our model can serve as a tool to forecast PWS under future climate and sea-level scenarios while planning hydrological restoration measures. Site-specific hydrological and climatic scenarios indicate that freshwater inflow and SLR are dominant drivers controlling PWS. Increasing freshwater (Scenario 1) can reduce PWS causing the expansion of freshwater and brackish vegetation and reducing mangrove area at the ecotone boundary. Seawater intrusion associated with SLR (Scenario 2) increases coastal groundwater discharge and salt concentration significantly, increasing PWS in all sites. Therefore, RHYMAN can help explore the hydrological and ecological outcomes (e.g., vegetation dominance) depending on the relative balance between net freshwater inflow and variable sea-level rise. Although RHYMAN simulations have provided evidence of the close balance between freshwater input and SLR, a landscape-level assessment is needed to understand if the mangrove-marsh ecotone region will be resilient to proposed hydrological management decisions (Danielson et al., 2017; Lugo, 1980; Rivera-Monroy et al., 2019) or if it is currently beyond a tipping point as CERP undergoes full implementation (National Academies of Sciences, 2016). Because hydrological restoration implies restoring freshwater flows to promote freshwater vegetation expansion and avoid, for example, “peat collapse” (Chambers et al., 2019; Ellison and Stoddart, 1991; Servais et al., 2020; Snedaker, 1995) as a result of saltwater intrusion, key restoration decisions are needed to continue the adaptative implementation and management of CERP (National Academies of Sciences, 2016). This includes the assessment of positive and negative environmental impacts and associated uncertainties of freshwater diversions in the context of climate change and mitigation plans in this unique oligotrophic karstic coastal region.

Declaration of Competing Interest

The authors declare that they have no known competing financial interests or personal relationships that could have appeared to influence the work reported in this paper.

Acknowledgments

This project was funded by the National Science Foundation (NSF) through the Florida Coastal Everglades Long-Term Ecological Research (FCE LTER) program (#DBI-0620409, #DEB-9910514) and the Department of the Interior South-Central Climate Adaptation Science Center (SC−CASC; Cooperative Agreement Grant #G12AC00002). Special thanks to the Everglades National Park for granting research permits and to the Florida Bay Interagency Science Center-Everglades National Park (FBISC-ENP) for logistic support during the study. This is contribution number 982 from the Southeast Environmental Research Center in the Institute of Environment at Florida International University. We thank Dr. Stephanie Romañach (USGS) and two anonymous reviewers for their constructive comments. This paper is part of a PhD dissertation to be submitted to the Department of Oceanography and Coastal Sciences, Louisiana State University by XZ. Any use of trade, firm, or product names is for descriptive purposes only and does not imply endorsement by the U.S. Government.

Supplementary materials

Supplementary material associated with this article can be found, in the online version, at doi:10.1016/j.ecolmodel.2020.109292.

Appendix A. Model parameterization

A.1. Forcing function parameters

Precipitation was considered as the major source of upland water surface flow into the study area. Throughfall represents the actual precipitation volume reaching the forest floor (~95% of total precipitation; Twilley and Chen, 1998). Thus, surface water flow was equal to daily average throughfall multiplied by a runoff coefficient (90%). Daily seepage was also a site-specific constant for each simulation and determined by water level records obtained at each site. When the water level was below soil surface and no precipitation occurred in one day, then seepage was considered as the difference between ET and the change in water level on that particular day (Twilley and Chen, 1998). Specific magnitudes are listed in **Table 2**.

A.2. Topographic and hydrological parameters

Three topographic parameters (**Table 2**), including ground relative surface level, bankfull stage, and edge threshold, characterize the local relative elevation settings at each study site. Ground surface level and bankfull stage were determined via sensitivity analysis, while edge threshold was site-specific; this parameter should be directly measured or determined by linear regression between water levels in the channel and inland forest when channel water floods the mangrove floor (e.g., Tsai, 2008). Particularly, given the relatively long study period (2004–2016), the ground surface level changed over years due to the sediment deposition/transportation associated with tidal exchange and storms; especially at the local/micro-scale. Additionally, the zero-marker of the channel water level data was changed in some years due to hurricane damage/re-installation. To

adjust these year-specific modifications, the ground surface level varied over the study period (Table 2). Hydrological parameters controlling water and salt exchange are site-specific or adapted from HYMAN and include specific yield for aboveground and underground water, salt content exported by channel water (tidal cycle) or surface flow, and precipitation canopy interception (Table 2).

Appendix B. Model initialization

RHYMAN includes the implementation of four main sub-routines given site differences in stages associated with channel and *in situ* water level and local topography (**Fig. S1, Fig. S2**).Before each simulation (one year), initial water level and PWS values were defined using December values from the previous year. Thus, RHYMAN first evaluates if the initial water level in the mangrove wetland is aboveground ("High Water") or belowground ("Low Water") (**Fig. S2**). The model then compares the channel water level to the edge threshold to determine the "actual" water level in the channel relative to the forest ground. Based on the "actual" water level in the channel, the model then determines if the soil is flooded ("Tide") or not ("NoTide") each day. Therefore, RHYMAN executes one sub-routine in one day to calculate water level, salt content, and PWS sequentially as influenced by each hydrological component as stated in the model description.

Appendix C. Sensitivity analysis

Sensitivity (S) was defined by the following equation:

$$S = [\Delta X_j/X_j]/[\Delta P_i/P] \tag{C1}$$

where P_i is the best estimate of a given parameter i, ΔP_i is the change in parameter i; X_j is the state variable j (i.e., PWS and water level), ΔX_j is the change in the j state variable caused by a change in the parameter i values. The higher the S absolute value of a given parameter, the more sensitive the model is to such parameter. Negative S represents the negative relationship between parameter change and the change in the state variable. Because the specific yield aboveground and precipitation interception value range from 0 to 1 (Table 2), we only calculated the S value with −25% change of the best estimate (0.95).

Appendix D. Statistical measures

D.1. Bias

The bias indicates the over- or under-estimate by comparing the simulated value to observations; it is the difference between the mean of simulated values and mean of observations:

$$Bias = \frac{\sum_{i=1}^{n}(S_i - O_i)}{n} \tag{D1}$$

where S_i and O_i are the simulated and observed values of state variables (i.e., water level and PWS) at each time; n is the total number of observations.

D.2. Coefficient of determination (R^2)

The coefficient of determination (R^2) represents the proportion of the variance in the observed variables that can be predicted from the simulated variable; it measures the linear regression between the simulated and observed values as defined by the following equation:

$$R^2 = \frac{[\sum_{i=1}^{n}(O_i - \bar{O})(S_i - \bar{S})]^2}{\sqrt{\sum_{i=1}^{n}(O_i - \bar{O})^2}\sqrt{\sum_{i=1}^{n}(S_i - \bar{S})^2}} \tag{D2}$$

D.3. Root mean square error (RMSE)

The root mean square error (RMSE) measures how much error is between simulated and observed values. The smaller the RMSE value is, the closer the simulated value is to the observation. The RMSE is calculated using the following equation:

$$RMSE = \sqrt{\frac{\sum_{i=1}^{n}(S_i - O_i)^2}{n}} \tag{D3}$$

D.4. Nash-Sutcliffe efficiency (NSE)

Nash-Sutcliffe efficiency (NSE) is defined as:

$$NSE = 1 - \frac{\sum_{i=1}^{n}(O_i - S_i)^2}{\sum_{i=1}^{n}(O_i - \bar{O})^2} \tag{D4}$$

The NSE determines the relative magnitude of the residual variance compared to the observed value variance. This efficiency ranges from -∞ to 1 and measure how well the regression between simulated and observed values is compared to 1:1 line. The negative value indicates that the mean of the observed values is a better predictor than the simulated value (Wang et al., 2012).

References

Alongi, D., 2009. The energetics of mangrove forests. Springer Science & Business Media.

Alongi, D.M., Christoffersen, P., Tirendi, F., 1993. The influence of forest type on microbial-nutrient relationships in tropical mangrove sediments. J. Exp. Mar. Biol. Ecol. 171, 201–223.

Ball, M.C., 1988a. Ecophysiology of mangroves. Trees-Struct. Funct. 2, 129–142.

Ball, M.C., 1988b. Salinity tolerance in the mangroves Aegiceras corniculatum and Avicennia marina. I. Water use in relation to growth, carbon partitioning, and salt balance. Funct. Plant Biol.15 447–464. https://doi.org/10.1071/pp9880447.

Ball, M.C., Pidsley, S.M., 1995. Growth-responses to salinity in relation to distribution of 2 mangrove species, Sonneratia-alba and S-lanceolata, in Northern Australia. Funct. Ecol. 9, 77–85. https://doi.org/10.2307/2390093.

Bouillon, S., Middelburg, J.J., Dehairs, F., Borges, A.V., Abril, G., Flindt, M.R., Ulomi, S., Kristensen, E., 2007. Importance of intertidal sediment processes and porewater exchange on the water column biogeochemistry in a pristine mangrove creek (Ras Dege, Tanzania).

Castañeda-Moya, E., Rivera-Monroy, V.H., Chambers, R.M., Zhao, X., Lamb-Wotton, L., Gorsky, A., Gaiser, E.E., Troxler, T.G., Kominoski, J.S., Hiatt, M., 2020. Hurricanes fertilize mangrove forests in the Gulf of Mexico (Florida Everglades, USA). Proc. Natl. Acad. Sci. U. S. A. 117, 4831–4841. https://doi.org/10.1073/pnas.1908597117.

Castañeda-Moya, E., Rivera-Monroy, V.H., Twilley, R.R., 2006. Mangrove zonation in the dry life zone of the Gulf of Fonseca, Honduras. Estuaries Coasts 29, 751–764. https://doi.org/10.1007/bf02786526.

Castañeda-Moya, E., Twilley, R.R., Rivera-Monroy, V.H., 2013. Allocation of biomass and net primary productivity of mangrove forests along environmental gradients in the Florida Coastal Everglades, USA. For. Ecol. Manage. 307, 226–241. https://doi.org/10.1016/j.foreco.2013.07.011.

Castañeda-Moya, E., Twilley, R.R., Rivera-Monroy, V.H., Marx, B.D., Coronado-Molina, C., Ewe, S.M., 2011. Patterns of root dynamics in mangrove forests along environmental gradients in the Florida Coastal Everglades. Ecosystems 14, 1178–1195.

Castañeda-Moya, E., Twilley, R.R., Rivera-Monroy, V.H., Zhang, K., Davis, S.E., Ross, M., 2010. Sediment and nutrient deposition associated with Hurricane Wilma in mangroves of the Florida Coastal Everglades. Estuaries Coasts 33, 45–58.

Chambers, L.G., Guevara, R., Boyer, J.N., Troxler, T.G., Davis, S.E., 2016. Effects of salinity and inundation on microbial community structure and function in a mangrove peat soil. Wetlands 36, 361–371.

Chambers, L.G., Steinmuller, H.E., Breithaupt, J.L., 2019. Toward a mechanistic understanding of "peat collapse" and its potential contribution to coastal wetland loss. Ecology 100, e02720.

Chen, R., Twilley, R.R., 1999. Patterns of mangrove forest structure and soil nutrient dynamics along the Shark River Estuary. Estuaries 22, 955–970. https://doi.org/10.2307/1353075.

Childers, D.L., 2006. A synthesis of long-term research by the Florida Coastal Everglades LTER Program. Hydrobiologia 569, 531–544.

Crase, B., Liedloff, A., Vesk, P.A., Burgman, M.A., Wintle, B.A., 2013. Hydroperiod is the main driver of the spatial pattern of dominance in mangrove communities. Glob. Ecol. Biogeog.22 806–817. https://doi.org/10.1111/geb.12063.

Dahl, K.A., Fitzpatrick, M.F., Spanger-Siegfried, E., 2017. Sea level rise drives increased tidal flooding frequency at tide gauges along the U.S. East and Gulf Coasts: projections for 2030 and 2045. PLoS ONE 12, e0170949. https://doi.org/10.1371/journal.pone.0170949.

Danielson, T.M., Rivera-Monroy, V.H., Castañeda-Moya, E., Briceño, H., Travieso, R., Marx, B.D., Gaiser, E., Farfán, L.M., 2017. Assessment of Everglades mangrove forest resilience: implications for above-ground net primary productivity and carbon dynamics. For. Ecol. Manage. 404, 115–125. https://doi.org/10.1016/j.foreco.2017.08.009.

Davey, M., Brookshaw, A., Ineson, S., 2014. The probability of the impact of ENSO on precipitation and near-surface temperature. Clim. Risk Manag.1 5–24.

Day, J.W., Coronado-Molina, C., Vera-Herrera, F.R., Twilley, R., Rivera-Monroy, V.H., Alvarez-Guillen, H., Day, R., Conner, W., 1996. A 7 year record of above-ground net primary production in a southeastern Mexican mangrove forest. Aquat. Bot. 55, 39–60. https://doi.org/10.1016/0304-3770(96)01063-7.

Dessu, S.B., Price, R.M., Troxler, T.G., Kominoski, J.S., 2018. Effects of sea-level rise and freshwater management on long-term water levels and water quality in the Florida Coastal Everglades. J. Environ. Manage. 211, 164–176. https://doi.org/10.1016/j.jenvman.2018.01.025.

Donato, D.C., Kauffman, J.B., Murdiyarso, D., Kurnianto, S., Stidham, M., Kanninen, M., 2011. Mangroves among the most carbon-rich forests in the tropics. Nat. Geosci. 4, 293–297. https://doi.org/10.1038/ngeo1123.

Duever, M., Meeder, J., Meeder, L., McCollom, J., 1994. The climate of south Florida and its role in shaping the Everglades ecosystem. Everglades 225–248.

Ellison, J.C., Stoddart, D.R., 1991. Mangrove ecosystem collapse during predicted sea-level rise - holocene analogs and implications. J. Coast. Res.7 151–165.

Enwright, N.M., Griffith, K.T., Osland, M.J., 2016. Barriers to and opportunities for landward migration of coastal wetlands with sea-level rise. Front. Ecol. Environ. 14, 307–316.

Ewe, S.M.L., Sternberg, L.D.S.L., Childers, D.L., 2007. Seasonal plant water uptake patterns in the saline southeast Everglades ecotone. Oecologia 152, 607–616. https://doi.org/10.1007/S00442-007-0699-X.

Feher, L.C., Osland, M.J., Anderson, G.H., Vervaeke, W.C., Krauss, K.W., Whelan, K.R., Balentine, K.M., Tiling-Range, G., Smith, T.J., Cahoon, D.R., 2019. The long-term effects of hurricanes Wilma and Irma on soil elevation change in Everglades mangrove forests. Ecosystems 1–15.

Flower, H., Rains, M., Carl Fitz, H, Orem, W, Newman, S, Osborne, T.Z, Ramesh Reddy, K, Obeysekera, J, 2019. Shifting ground: landscape-scale modeling of biogeochemical processes under climate change in the Florida Everglades. Environ. Manage. 64, 416–435. https://doi.org/10.1007/s00267-019-01200-8.

Flower, H., Rains, M., Fitz, C., 2017. Visioning the future: scenarios modeling of the Florida Coastal Everglades. Environ. Manage. 60, 989–1009. https://doi.org/10.1007/s00267-017-0916-2.

Friess, D.A., Watson, J.G, 2016. Inundation classes, and their influence on paradigms in mangrove forest ecology. Wetlands 37, 603–613. https://doi.org/10.1007/s13157-016-0747-6.

Giri, C., Ochieng, E., Tieszen, L.L., Zhu, Z., Singh, A., Loveland, T., Masek, J., Duke, N., 2011. Status and distribution of mangrove forests of the world using earth observation satellite data. Glob. Ecol. Biogeog.20 154–159. https://doi.org/10.1111/j.1466-8238.2010.00584.x.

Guo, H., Weaver, C., Charles, S.P., Whitt, A., Dastidar, S., D'Odorico, P., Fuentes, J.D., Kominoski, J.S., Armitage, A.R., Pennings, S.C., 2017. Coastal regime shifts: rapid responses of coastal wetlands to changes in mangrove cover. Ecology 98, 762–772. https://doi.org/10.1002/ecy.1698.

Habib, E., Larson, B.F., Nuttle, W.K., Rivera-Monroy, V.H., Nelson, B.R., Meselhe, E.A., Twilley, R.R., 2008. Effect of rainfall spatial variability and sampling on salinity prediction in an estuarine system. J. Hydrol. (Amst.) 350, 56–67. https://doi.org/10.1016/j.jhydrol.2007.11.034.

Habib, E., Nuttle, W.K., Rivera-Monroy, V.H., Gautam, S., Wang, J., Meselhe, E., Twilley, R.R., 2007. Assessing effects of data limitations on salinity forecasting in Barataria Basin, Louisiana, with a bayesian analysis. J. Coast. Res.233 749–763. https://doi.org/10.2112/06-0723.1.

Han, X., Feng, L., Hu, C., Kramer, P., 2018. Hurricane-induced changes in the Everglades National Park Mangrove Forest: landsat observations between 1985 and 2017. J. Geophys. Res. 123, 3470–3488. https://doi.org/10.1029/2018jg004501.

He, D., Rivera-Monroy, V.H., Jaffé, R., Zhao, X., 2020. Mangrove leaf species-specific isotopic signatures along a salinity and phosphorus soil fertility gradients in a subtropical estuary. Estuar. Coast. Shelf Sci., 106768.

Howard, R.J., Day, R.H., Krauss, K.W., From, A.S., Allain, L., Cormier, N., 2017. Hydrologic restoration in a dynamic subtropical mangrove-to-marsh ecotone. Restor. Ecol.25 471–482. https://doi.org/10.1111/rec.12452.

Howard, R.J., From, A.S., Krauss, K.W., Andres, K.D., Cormier, N., Allain, L., Savarese, M., 2020. Soil surface elevation dynamics in a mangrove-to-marsh ecotone characterized by vegetation shifts. Hydrobiologia 1–20.

Jerath, M., Bhat, M., Rivera-Monroy, V.H., Castañeda-Moya, E., Simard, M., Twilley, R.R., 2016. The role of economic, policy, and ecological factors in estimating the value of carbon stocks in Everglades mangrove forests, South Florida. Environ. Sci. Policy 66, 160–169. https://doi.org/10.1016/j.envsci.2016.09.005.

Jørgensen, S.E., Fath, B.D., 2011. Concepts of modelling. In: Jørgensen, S.E, Fath, B.D (Eds.), Applications in Environmental Management and Research 23. Elsevier, pp. 19–93. https://doi.org/10.1016/b978-0-444-53567-2.00002-8.

Kauffman, J.B., Bhomia, R.K., 2017. Ecosystem carbon stocks of mangroves across broad environmental gradients in West-Central Africa: global and regional comparisons. PLoS ONE 12, e0187749. https://doi.org/10.1371/journal.pone.0187749.

Krauss, K.W., Doyle, T.W., Twilley, R.R., Rivera-Monroy, V.H., Sullivan, J.K., 2006. Evaluating the relative contributions of hydroperiod and soil fertility on growth of south Florida mangroves. Hydrobiologia 569, 311–324. https://doi.org/10.1007/s10750-006-0139-7.

Krauss, K.W., Lovelock, C.E., McKee, K.L., Lopez-Hoffman, L., Ewe, S.M.L., Sousa, W.P., 2008. Environmental drivers in mangrove establishment and early development: a review. Aquat. Bot. 89, 105–127.

Kristensen, E., Connolly, R.M., Otero, X.L., Marchand, C., Ferreira, T.O., Rivera-Monroy, V.H., 2017. Biogeochemical cycles: global approaches and perspectives. In: Rivera-Monroy, V.H, Lee, S.Y, Kristensen, E, Twilley, R.R (Eds.), Mangrove Ecosystems: A Global Biogeographic Perspective. Springer International Publishing, Cham, pp. 163–209. https://doi.org/10.1007/978-3-319-62206-4_6.

Lagomasino, D., Fatoyinbo, T., Castañeda-Moya, E., Cook, B., Montesano, P., Neigh, C., Ott, L., Chavez, S., Morton, D., 2020. Storm surge, not wind, caused mangrove dieback in southwest Florida following Hurricane Irma.

Lagomasino, D., Price, R.M., Herrera-Silveira, J., Miralles-Wilhelm, F., Merediz-Alonso, G., Gomez-Hernandez, Y., 2015. Connecting groundwater and surface water sources in groundwater dependent coastal wetlands and estuaries: sian Ka'an Biosphere Reserve, Quintana Roo. Estuaries Coasts 38, 1744–1763.

Langevin, C., Swain, E., Wolfert, M., 2005. Simulation of integrated surface-water/ground-water flow and salinity for a coastal wetland and adjacent estuary. J. Hydrol. (Amst.) 314, 212–234.

Lara, R.J., Cohen, M.C., 2006. Sediment porewater salinity, inundation frequency and mangrove vegetation height in Bragança, North Brazil: an ecohydrology-based empirical model. Wetlands Ecol. Manag.14 349–358.

Larsen, L., Aumen, N., Bernhardt, C., Engel, V., Givnish, T., Hagerthey, S., Harvey, J., Leonard, L., McCormick, P., McVoy, C., Noe, G., Nungesser, M., Rutchey, K., Sklar, F., Troxler, T., Volin, J., Willard, D., 2011. Recent and historic drivers of landscape change in the Everglades Ridge, Slough, and Tree Island Mosaic. Crit. Rev. Environ. Sci. Technol. 41, 344–381. https://doi.org/10.1080/10643389.2010.531219.

Larsen, L.G., Choi, J., Nungesser, M.K., Harvey, J.W., 2012. Directional connectivity in hydrology and ecology. Ecol. Appl. 22, 2204–2220. https://doi.org/10.1890/11-1948.1.

Larsen, L.G., Harvey, J.W., 2010. How vegetation and sediment transport feedbacks drive landscape change in the Everglades and wetlands worldwide. Am. Nat. 176, E66–E79.

Lee, R.Y., Porubsky, W.P., Feller, I.C., McKee, K.L., Joye, S.B., 2008. Porewater biogeochemistry and soil metabolism in dwarf red mangrove habitats (Twin Cays, Belize). Biogeochemistry 87, 181–198.

Leopold, A., Marchand, C., Deborde, J., Allenbach, M., 2017. Water biogeochemistry of a mangrove-dominated estuary under a semi-arid climate (New Caledonia). Estuaries Coasts 40, 773–791.
Lugo, A.E., 1980. Mangrove ecosystems: successional or steady state? Biotropica 12, 65–72. https://doi.org/10.2307/2388158.
Lugo, A.E., Medina, E., 2014. Mangrove forests. Pages 343-352 in Encyclopedia of Natural Resources-Land 1 Taylor and Francis, New York.
Lugo, A.E., Snedaker, S.C., 1974. The ecology of mangroves. Annu. Rev. Ecol. Syst. 5, 39–64. https://doi.org/10.1146/annurev.es.05.110174.000351.
Mazda, Y., Ikeda, Y., 2006. Behavior of the groundwater in a riverine-type mangrove forest. Wetlands Ecol. Manag.14 477–488.
Mazda, Y., Kanazawa, N., Wolanski, E., 1995. Tidal asymmetry in mangrove creeks. Hydrobiologia 295, 51–58. https://doi.org/10.1007/BF00029110.
Mazda, Y., Kobashi, D., Okada, S., 2005. Tidal-scale hydrodynamics within mangrove swamps. Wetlands Ecol. Manag.13 647–655.
McKee, K.L., Mendelssohn, I.A., Hester, M.W., 1988. Reexamination of pore water sulfide concentrations and redox potentials near the aerial roots of Rhizophora mangle and Avicennia germinans. Am. J. Bot. 75, 1352–1359.
McKee, K.L., Vervaeke, W.C., 2018. Will fluctuations in salt marsh-mangrove dominance alter vulnerability of a subtropical wetland to sea-level rise? Glob. Chang. Biol. 24, 1224–1238. https://doi.org/10.1111/gcb.13945.
McKee, M., White, J., Putnam-Duhon, L., 2016. Simulated storm surge effects on fresh-water coastal wetland soil porewater salinity and extractable ammonium levels: implications for marsh recovery after storm surge. Estuar. Coast. Shelf Sci. 181, 338–344.
Michot, B.D., Meselhe, E.A., Krauss, K.W., Shrestha, S., From, A.S., Patino, E., 2017. Hydrologic modeling in a Marsh–mangrove ecotone: predicting wetland surface water and salinity response to restoration in the ten thousand islands region of Florida. J. Hydrol. Eng. 22. https://doi.org/10.1061/(asce)he.1943-5584.0001260.
Mitsch, W.J., Gosselink, J.G., 2007. Wetlands. John Wiley & Sons, Inc, Hoboken.
Morris, J.T., 1995. The mass balance of salt and water in intertidal sediments: results from North Inlet. Estuaries 18, 556–567. https://doi.org/10.2307/1352376.
National Academies of Sciences, Engineering, and Medicine, 2016. Progress Toward Restoring the Everglades: The Sixth Biennial Review-2016. National Academies Press, Washington, DC. https://www.nap.edu/catalog/23672/progress-toward-restoring-the-everglades-the-sixth-biennial-review-2016.
Nuttle, W.K., Fourqurean, J.W., Cosby, B.J., Zieman, J.C., Robblee, M.B., 2000. Influence of net freshwater supply on salinity in Florida Bay. Water Resour. Res. 36, 1805–1822. https://doi.org/10.1029/1999wr900352.
Ochoa-Gómez, J.G., Serviere-Zaragoza, E., Lluch-Cota, D.B., Rivera-Monroy, V.H., Oechel, W., Troyo-Diéguez, E., Lluch-Cota, S.E., 2018. Structural complexity and biomass of arid zone mangroves in the southwestern Gulf of California: key factors that influence fish assemblages. J. Coast. Res.34 979–986.
Odum, H.T., 1983. Systems ecology; an introduction.
Osland, M.J., Enwright, N., Day, R.H., Doyle, T.W., 2013. Winter climate change and coastal wetland foundation species: salt marshes vs. mangrove forests in the south-eastern United States. Glob. Chang. Biol. 19, 1482–1494. https://doi.org/10.1111/gcb.12126.
Price, R.M., Swart, P.K., Fourqurean, J.W., 2006. Coastal groundwater discharge–an additional source of phosphorus for the oligotrophic wetlands of the Everglades. Hydrobiologia 569, 23–36.
Price, R.M., Top, Z., Happell, J.D., Swart, P.K., 2003. Use of tritium and helium to define groundwater flow conditions in Everglades National Park. Water Resour. Res. 39. https://doi.org/10.1029/2002wr001929.
Provost, M.W., 1973. Mean high water mark and use of tidelands in Florida. Scientist 50–66.
Rivera-Monroy, V.H., Danielson, T.M., Castañeda-Moya, E., Marx, B.D., Travieso, R., Zhao, X., Gaiser, E.E., Farfan, L.M., 2019. Long-term demography and stem productivity of Everglades mangrove forests (Florida, USA): resistance to hurricane disturbance. For. Ecol. Manage. 440, 79–91. https://doi.org/10.1016/j.foreco.2019.02.036.
Rivera-Monroy, V.H., Osland, M.J., Day, J.W., Ray, S., Rovai, A., Day, R.H., Mukherjee, J., 2017. Advancing mangrove macroecology. Mangrove Ecosystems: A Global Biogeographic Perspective. Springer, pp. 347–381. https://link.springer.com/chapter/10.1007%2F978-3-319-62206-4_11
Rivera-Monroy, V.H., Twilley, R.R., Davis, S.E., Childers, D.L., Simard, M., Chambers, R., Jaffe, R., Boyer, J.N., Rudnick, D.T., Zhang, K., Castañeda-Moya, E., Ewe, S.M.L., Price, R.M., Coronado-Molina, C., Ross, M., Smith, T.J., Michot, B., Meselhe, E., Nuttle, W., Troxler, T.G., Noe, G.B., 2011. The role of the Everglades Mangrove Ecotone Region (EMER) in regulating nutrient cycling and wetland productivity in South Florida. Crit. Rev. Environ. Sci. Technol. 41, 633–669. https://doi.org/10.1080/10643389.2010.530907.
Rivera-Monroy, V.H., Twilley, R.R., Medina, E., Moser, E.B., Botero, L., Francisco, A.M., Bullard, E., 2004. Spatial variability of soil nutrients in disturbed riverine mangrove forests at different stages of regeneration in the San Juan River estuary. Estuaries 27, 44–57. https://doi.org/10.1007/bf02803559.
Romañach, S.S., Beerens, J.M., Patton, B.A., Chapman, J.P., Hanson, M.R., 2019. Impacts of saltwater intrusion on wetland prey production and composition in a historically freshwater Marsh. Estuaries Coasts 42, 1600–1611.
Ross, M.S., Meeder, J.F., Sah, J.P., Ruiz, P.L., Telesnicki, G.J., 2000. The Southeast Saline Everglades revisited: 50 years of coastal vegetation change. J. Veg. Sci.11 101–112. https://doi.org/10.2307/3236781.
Rovai, A., Riul, P., Twilley, R., Castañeda-Moya, E., Rivera-Monroy, V., Williams, A., Simard, M., Cifuentes-Jara, M., Lewis, R., Crooks, S., 2016. Scaling mangrove aboveground biomass from site-level to continental-scale. Glob. Ecol. Biogeog.25 286–298.
Rovai, A.S., Twilley, R.R., Castañeda-Moya, E., Riul, P., Cifuentes-Jara, M., Manrow-Villalobos, M., Horta, P.A., Simonassi, J.C., Fonseca, A.L., Pagliosa, P.R., 2018. Global controls on carbon storage in mangrove soils. Nat. Clim. Chang. 8, 534–538. https://doi.org/10.1038/s41558-018-0162-5.
Saha, A.K., Moses, C.S., Price, R.M., Engel, V., Smith, T.J., Anderson, G., 2012. A hydrological budget (2002-2008) for a large subtropical wetland ecosystem indicates marine groundwater discharge accompanies diminished freshwater flow. Estuaries and Coasts 35, 459–474. https://doi.org/10.1007/s12237-011-9454-y.
Saha, A.K., Saha, S., Sadle, J., Jiang, J., Ross, M.S., Price, R.M., Sternberg, L.S.L.O., Wendelberger, K.S., 2011. Sea level rise and South Florida coastal forests. Clim. Chang.107 81–108. https://doi.org/10.1007/s10584-011-0082-0.
Saintilan, N., Wilson, N.C., Rogers, K., Rajkaran, A., Krauss, K.W., 2014. Mangrove expansion and salt marsh decline at mangrove poleward limits. Glob. Chang. Biol. 20, 147–157. https://doi.org/10.1111/gcb.12341.
Santos, I.R., Maher, D.T., Larkin, R., Webb, J.R., Sanders, C.J., 2019. Carbon outwelling and outgassing vs. burial in an estuarine tidal creek surrounded by mangrove and saltmarsh wetlands. Limnol. Oceanogr. 64, 996–1013. https://doi.org/10.1002/lno.11090.
Servais, S., Kominoski, J.S., Coronado-Molina, C., Bauman, L., Davis, S.E., Gaiser, E.E., Kelly, S., Madden, C., Mazzei, V., Rudnik, D., 2020. Effects of saltwater pulses on soil microbial enzymes and organic matter breakdown in freshwater and Brackish coastal wetlands. Estuaries Coasts 1–17.
Sherman, R.E., Fahey, T.J., Howarth, R.W., 1998. Soil-plant interactions in a neotropical mangrove forest: iron, phosphorus and sulfur dynamics. Oecologia 115, 553–563. https://doi.org/10.1007/s004420050553.
Simard, M., Fatoyinbo, L., Smetanka, C., Rivera-Monroy, V.H., Castañeda-Moya, E., Thomas, N., Van der Stocken, T., 2019. Mangrove canopy height globally related to precipitation, temperature and cyclone frequency. Nat. Geosci. 12, 40–45. https://doi.org/10.1038/s41561-018-0279-1. https://www.nature.com/articles/s41561-018-0279-1#citeas.
Simard, M., Zhang, K., Rivera-Monroy, V.H., Ross, M.S., Ruiz, P.L., Castañeda-Moya, E., Twilley, R.R., Rodriguez, E., 2006. Mapping height and biomass of mangrove forests in Everglades National Park with SRTM elevation data. Photogram. Eng. Rem. Sens.72 299–311. https://doi.org/10.14358/pers.72.3.299.
Sklar, F.H., Chimney, M.J., Newman, S., McCormick, P., Gawlik, D., Miao, S., McVoy, C., Said, W., Newman, J., Coronado, C., 2005. The ecological–societal underpinnings of Everglades restoration. Front. Ecol. Environ. 3, 161–169.
Smith, C.G., Price, R.M., Swarzenski, P.W., Stalker, J.C., 2016. The role of ocean tides on groundwater-surface water exchange in a mangrove-dominated estuary: shark River Slough, Florida Coastal Everglades. Estuaries Coasts 39, 1600–1616. https://doi.org/10.1007/s12237-016-0079-z.
Smith, T.J., Anderson, G.H., Balentine, K., Tiling, G., Ward, G.A., Whelan, K.R.T., 2009. Cumulative impacts of hurricanes on Florida mangrove ecosystems: sediment deposition, storm surges and vegetation. Wetlands 29, 24–34.
Snedaker, S.C., 1995. Mangroves and climate change in the Florida and Caribbean region: scenarios and hypotheses. Hydrobiologia 295, 43–49. https://doi.org/10.1007/bf00029109.
Tait, D.R., Maher, D.T., Macklin, P.A., Santos, I.R., 2016. Mangrove pore water exchange across a latitudinal gradient. Geophys. Res. Lett. 43, 3334–3341. https://doi.org/10.1002/2016gl068289.
Tait, D.R., Maher, D.T., Sanders, C.J., Santos, I.R., 2017. Radium-derived porewater exchange and dissolved N and P fluxes in mangroves. Geochim. Cosmochim. Ac. 200, 295–309. https://doi.org/10.1016/j.gca.2016.12.024.
Thomson, R.E., Emery, W.J., 2014. Data analysis methods in physical oceanography. Newnes.
Tobias, C.R., Harvey, J.W., Anderson, I.C., 2001. Quantifying groundwater discharge through fringing wetlands to estuaries: seasonal variability, methods comparison, and implications for wetland-estuary exchange. Limnol. Oceanogr. 46, 604–615. https://doi.org/10.4319/lo.2001.46.3.0604.
Tomlinson, P.B., 2016. The Botany of Mangroves. Cambridge University Press.
Troxler, T.G., Barr, J.G., Fuentes, J.D., Engel, V., Anderson, G., Sanchez, C., Lagomasino, D., Price, R., Davis, S.E., 2015. Component-specific dynamics of riverine mangrove CO2 efflux in the Florida coastal Everglades. Agric. For. Meteorol. 213, 273–282.
Troxler, T.G., Childers, D.L., Madden, C.J., 2013. Drivers of decadal-scale change in Southern Everglades wetland macrophyte communities of the coastal ecotone. Wetlands 34, 81–90. https://doi.org/10.1007/s13157-013-0446-5.
Tsai, C.-F., 2008. Application of the HYMAN model to evaluate the water and salt budgets in three mangrove sites along Shark River. Everglades.
Twilley, R.R., Castañeda-Moya, E., Rivera-Monroy, V.H., Rovai, A., 2017. Productivity and carbon dynamics in mangrove wetlands. Mangrove ecosystems: a global biogeographic perspective. Springer, pp. 113–162. https://link.springer.com/chapter/10.1007/978-3-319-62206-4_5
Twilley, R.R., Chen, R., 1998. A water budget and hydrology model of a basin mangrove forest in Rookery Bay. Mar. Freshwater Res. 49, 309–323. https://doi.org/10.1071/mf97220.
Twilley, R.R., Rivera-Monroy, V.H., 2005. Developing performance measures of mangrove wetlands using simulation models of hydrology, nutrient biogeochemistry, and community dynamics. J. Coast. Res. 79–93.
van der Valk, A.G., Wetzel, P., Cline, E., Sklar, F.H., 2008. Restoring tree islands in the Everglades: experimental studies of tree seedling survival and growth. Restor. Ecol.16 281–289. https://doi.org/10.1111/j.1526-100X.2007.00311.x.
van Maanen, B., Coco, G., Bryan, K.R., 2015. On the ecogeomorphological feedbacks that control tidal channel network evolution in a sandy mangrove setting. Proc. Math. Phys. Eng. Sci. 471, 20150115. https://doi.org/10.1098/rspa.2015.0115.
Wang, H., Hsieh, Y.P., Harwell, M.A., Huang, W., 2007. Modeling soil salinity distribution along topographic gradients in tidal salt marshes in Atlantic and Gulf coastal regions.

Ecol. Model. 201, 429–439.
Wang, H., Krauss, K.W., Noe, G.B., Stagg, C.L., Swarzenski, C.M., Duberstein, J.A., Conner, W.H., DeAngelis, D.L., 2020. Modeling soil porewater salinity response to drought in tidal freshwater forested wetlands. J. Geophys. Res.
Wang, H., Meselhe, E.A., Waldon, M.G., Harwell, M.C., Chen, C., 2012. Compartment-based hydrodynamics and water quality modeling of a Northern Everglades Wetland. Ecol. Model. 247, 273–285. https://doi.org/10.1016/j.ecolmodel.2012.09.007.
Wdowinski, S., Bray, R., Kirtman, B.P., Wu, Z., 2016. Increasing flooding hazard in coastal communities due to rising sea level: case study of Miami Beach. Ocean Coast. Manag. 126, 1–8. https://doi.org/10.1016/j.ocecoaman.2016.03.002.
Whelan, K.R.T., 2005. The Successional Dynamics of Lightning-Initiated Canopy Gaps in the Mangrove Forests of Shark River, Everglades National Park, USA. Florida International University, Miami, Fla, USA.
Wilensky, U., 1999. Center for connected learning and computer-based modeling. Netlogo. Northwestern University.
Woodroffe, C.D., 2002. Coasts: form, process and evolution. Cambridge University Press.
Wu, Y., Falconer, R.A., Struve, J., 2001. Mathematical modelling of tidal currents in mangrove forests. Environ. Model. Softw.16 19–29.
Yao, Q., Liu, K.B., 2017. Dynamics of marsh-mangrove ecotone since the mid-Holocene: a palynological study of mangrove encroachment and sea level rise in the Shark River Estuary. PLoS ONE 12, e0173670. https://doi.org/10.1371/journal.pone.0173670.
Yao, Q., Liu, K.B., Platt, W.J., Rivera-Monroy, V.H., 2015. Palynological reconstruction of environmental changes in coastal wetlands of the Florida Everglades since the mid-Holocene. Quat. Res. 83, 449–458. https://doi.org/10.1016/j.yqres.2015.03.005.